Leveraging Crosslinker Diffusion to Template Stiffness Gradients in Alginate Hydrogels

Zoe Ostrowski[1*], Tyler Price[1,2*], Juntao Zhang[3], Azarnoosh Foroozandehfar[1], Fred R. Namanda[4], Tim Kaufmann[1], Natalia Judka[1], Tyler Gardner[1], Mary Thatcher[1], Emmaline Miller[5], Lily Mesyk[1,6], Abigail Koep[1], Adam T. Melvin[5,7], Juan Ren[3] and Ian C. Schneider[1,8‡]

[1]Department of Chemical and Biological Engineering, Iowa State University
[2]Current address: Beckman Institute for Advanced Science and Technology and Department of Materials Science and Engineering, University of Illinois Urbana-Champaign
[3]Department of Mechanical Engineering, Iowa State University
[4]Molecular, Cellular and Developmental Biology Program, Iowa State University
[5]Cain Department of Chemical Engineering, Louisiana State University
[6]Current address: Department of Biochemistry, Bethel University
[7]Department of Chemical and Biomolecular Engineering, Clemson University
[8]Department of Genetics, Development and Cell Biology, Iowa State University

Present address: Iowa State University, Department of Chemical and Biological Engineering, 2114 Sweeney Hall, Ames, IA, 50011-2230
*Joint First Author
‡Author for correspondence (phone: (515) 294-0450, fax: (515) 294-2689, e-mail: ians@iastate.edu)

Abstract (242 words):

Mechanobiology drives many important cell biological behaviors such as stem cell differentiation, cancer drug resistance and cell migration up stiffness gradients, a process called durotaxis. The development of 3D hydrogel systems with tunable 2D mechanical gradient patterns affords the ability to study these mechanosensitive cell behaviors to understand cancer invasion or enhance wound healing through directed migration. In this paper, we developed an approach to spatially imprint within alginate hydrogels, gradients in mechanical properties that can be used to probe mechanobiology. Stencils were easily designed and fabricated using a common craft cutter to control the presentation of a calcium crosslinking solution to alginate gels. Different stencil shapes result in different gradients in opacity that can be imprinted into both thick and thin alginate gels of arbitrary 2D shape. The steepness of the opacity gradient as well as the maximum opacity can be controlled based on reproducible crosslinking kinetics regulated through calcium concentration and gradient developing time. Calcium crosslinking results in both opacity changes as well as increases in elastic modulus in the bulk hydrogel. Opacity correlates with elastic modulus, allowing it to be used as a proxy for local elastic modulus. Functionalized alginate gels with collagen and imprinting stiffness gradients within them resulted in cell invasion that was spatially dependent, where stiffer regions facilitated deeper invasion of breast cancer cells. Consequently, this stenciling approach represents a facile way to control stiffness gradients in alginate gels in order to study mechanosensitive cellular behavior.

Graphical Abstract:

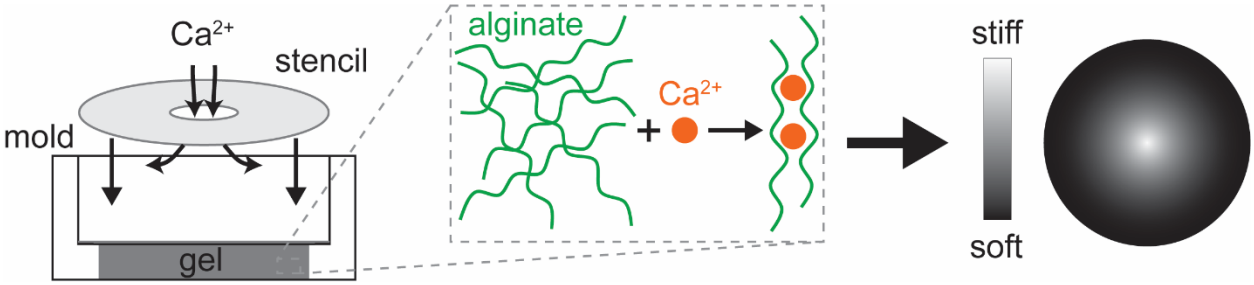

Key Words:

Stencil, craft cutter, alginic, opacity, durotaxis, mechanotaxis, cancer invasion

Abbreviations:

ECM: extracellular matrix

UV: ultraviolet

VIS: visible

PBS: phosphate buffered saline

DMEM: Dulbecco's modified Eagle medium

FBS: fetal bovine serum

APTES: aminoproplytriethoxysilane

NHS: N-hydroxysuccinimide

EDC: 1-ethyl-3-(3-dimethylaminopropyl) carbodiimide

FTIR: Fourier transform infrared

ATR: Attenuated total reflectance

4NB: 4-nitrobenzaldeyhde

AFM: Atomic force microscopy

MES: 2-(*N*-morpholino) ethanesulfonic acid

EGTA: Ethylene Glycol Tetraacetic Acid

TBS: Tris Buffered Saline

STED: Stimulated Emission Depletion

1. Introduction:

It is well-established that a wide variety of biological processes are driven by mechanobiology. These processes include development[1], immune response[2], wound healing[3] as well as diseases like cancer[4] and fibrosis[5]. Cells sense the stiffness of their environment, altering cell differentiation, drug sensitivity, metabolism and cell migration. Spatial gradients in stiffness formed in biomaterials allow for the study of these cell behaviors. Spatial gradients can reveal non-linear relationships between stiffness and the above mentioned cell behaviors along with the transcriptional, signaling and epigenetic signatures in ways that would be difficult to observe in individual experiments[6–9]. Furthermore, the ability to control gradients in stiffness is absolutely critical for understanding and controlling cell migration through durotaxis[1,10–13], directed cell migration in response to stiffness gradients. Durotaxis drives cancer metastasis as well as stromal cell invasion of the tumor[11]. Furthermore, durotaxis drives wound healing, where stiffness gradients in the wound bed are present and can recruit fibroblasts, organize wound contraction and facilitate hair follicle development[14]. Encoding these types of mechanical property gradients within biomaterials that are provisionally placed in the wound bed will likely lead to enhanced migration and faster wound healing, particularly in traumatic or chronic wounds.

A variety of biomaterials have been used as wound dressings, but the focus of these materials has been on absorption of exudate, maintenance of wound moisture or inhibition of microbial growth[15]. Alginate hydrogels are commonly used in wound dressings[16]. Alginate is a naturally occurring polymer derived from brown algae. Due to its biocompatibility, low toxicity, and structure similarity to extracellular matrices, it is becoming more commonly used in hydrogels for advanced wound dressings[17]. The stiffness of alginate hydrogels can be tuned by crosslinking them with divalent ions like calcium, allowing one to match hydrogel stiffness with tissue stiffness[18,19]. However sophisticated hydrogels with arbitrary stiffness gradients that could direct cells to particular targets within the wound bed at a faster rate have not been developed. In order to study the cellular and molecular mechanisms of cell migration that are present during wound healing or to generate tissue engineering constructs that can direct cells at high speed to targets, approaches for controlling gradients within hydrogels will need to be developed.

There are many ways to form biological gradients[20]. The most commonly used hydrogel system in which to generate mechanical property gradients and study mechanobiology or durotaxis is polyacrylamide. Stiffness gradients can be generated easily using designed masks and photoinitiators[21]. However, while polyacrylamide is a good model hydrogel system, cells cannot be readily embedded within it due to toxicity issues during polymerization and cell invasion is stunted due to an inability for cells to remodel this hydrogel, making its use difficult *in vivo*. Another common system in which to generate stiffness gradients is PEG-polymer systems[6,9], however these can be expensive due to the cost

of functionalized PEG. Stiffness gradients in collagen can be generated in collagen gels as well, however, these spatial gradients are usually accompanied by fiber alignment gradients[22]. Alginate hydrogels overcome these problems as they are relatively simple and inexpensive to fabrication. There are several examples of approaches that can generate alginate gradients. Gradients in stiffness have been generated through attachment to stiff interfaces[18,23], using dipping methods[24] or by merging two different alginate solutions, creating a gradient between the two[25]. However, these approaches are limited in the shape of gradients that can be generated. Bioprinting has been used to make gradients in alginate[26,27]. However, while bioprinting is becoming much more accessible for labs, it still requires relatively expensive equipment and optimization. Photopolymerization of alginate can be performed using methacrylated alginate and photoinitiators[28] or photocrosslinking of alginate using embedded vesicles that can release calcium[29]. However, while these approaches afforded very good spatial control and even allowed for temporal control, they either used reagents that can be cytotoxic or difficult to produce. What is needed in order to form stiffness gradients in hydrogels to study mechanobiological responses of cells is a system that can generate a wide variety of gradients, does not require expensive equipment and is easy to use.

Here we develop a stenciling method that can generate unique and tunable stiffness gradients within alginate hydrogels leveraging the controlled diffusion of calcium into the gel. The stencils are easily designed and fabricated, producing a variety of patterns. We show that calcium cross-links the alginate, resulting in an opacity change due to local polymer contraction or densification and enhanced light scattering. We have generated different gradient patterns in both thick and thin systems and characterized the kinetics of crosslinking. Bulk mechanical property measurements have been made and we have spatially mapped mechanical properties to the spatial position and have correlated this to changes in opacity. Finally, to we have demonstrated a spatially controlled cell biological response, cancer cell invasion, demonstrating the utility of forming these gradients in mechanical properties. This technique allows for the easy design and fabrication of alginate gels with tunable stiffness gradients.

2. Materials and Methods:

2.1 Assembly of stenciled alginate hydrogels

A custom 1-inch diameter mold with a 15.4-mm diameter hole was filled with 1 ml of an alginate gel containing 20 mg/ml alginate (alginic acid sodium salt from brown algae, Sigma Aldrich, low viscosity, MW ~ 30-100 kDa, A1112) and 20 mM calcium sulfate ($CaSO_4$, Acros Organics, 385351000). Additional buffers were used to dissolve the alginate and $CaSO_4$ including phosphate buffer saline (PBS) lacking magnesium and calcium (Gibco, 14190144) and Dulbecco's Modified Eagle's medium (DMEM, Sigma Aldrich, D6546) with 1% penicillin-streptomycin (Gibco, 15140122) and 10% heat-inactivated fetal bovine serum (FBS, Gibco, A5256801). A custom cut stencil is placed on top of the gel and sealed to the edge of the mold with vacuum grease (Dow Corning). Stencils are cut on transparency paper (Apollo Write on Transparency Film Clear) using a Cricut Maker 3. The Cricut Maker 3 allows for creation or uploading of any custom designs, shapes and text and has a spatial resolution of 1 mm diameter for the circle design (**Supplementary Figure 1**). All stencils have an overall diameter of 1 inch to fit the diameter of the mold. The smaller circle stencil has a diameter of 2.5 mm. The larger circle stencil has a diameter of 5 mm. The line stencil has a width of 1 mm, and the S shape stencil has a width of 3 mm. On top of the stencil is a solution of 80 mM $CaCl_2$ ($CaCl_2$ Fisher Scientific, C79) (**Figure 1A**). Thin alginate gels were generated using a mold cut using the Cricut Maker 3. Two layers of 1 mm thick silicone attached by two-sided adhesive were stacked together to create a chamber for a thin alginate gel. Thin alginate gels were made with final concentrations of 20 mg/ml alginate and 20 mM $CaSO_4$. A stencil made from transparent cellulose acetate was placed on top of the alginate gel, and 80 mM $CaCl_2$ filled the 35 mm cell culture dish (**Figure 2A**). Images were taken every five minutes for 8 h.

2.2 Fabrication of 3D-printed imaging chambers

A 3D printed imaging chamber was fabricated and adhered directly to a glass slide. The 3D printed imaging chambers were designed in SOLIDWORKS CAD software (3DS, Paris, France) and printed using Overture PLA (polylactic acid) 1.75 mm diameter filament with the Creality Ender-3 V2 3D printer. The .stl files from SOLIDWORKS were converted to .gcodes formed for printing in the slicing software Simplify3D (Simplify3D, Cincinnati, OH, USA). Two varieties of imaging chamber were fabricated: thin and thick. Both thin and thick chambers were printed with an imaging aperture dimension of 18 mm in diameter, an interior shelf width of 3 mm, a wall thickness of 1 mm, for a total diameter of 28 mm. Thin chambers had a total wall height of 5 mm, including the interior shelf thickness of 2 mm whereas thick chambers had a total wall height of 8 mm, including the interior shelf thickness of 4 mm. After printing the imaging chambers were removed from the printer bed and adhered to a 75 mm x 25 mm x 1 mm glass slide using vacuum grease. This forms the completed imaging chamber-slide complex that allows for the visualization using light microscopy.

157 **2.3 Imaging and image analysis of alginate gels**

158 Alginate gels were imaged using a home-built system including an 8-bit video camera (Javelin CCD) over
159 a period of 8 h with images taken every 5 min. The initial image of the gel was taken immediately before
160 80 mM $CaCl_2$ was placed on top of the stencil. Using ImageJ, the change in opacity (intensity) was
161 measured as a change in gray value at three locations on each gel: the center of the stencil, 1 mm from the
162 edge of the stencil and 3 mm from the edge of the stencil. The intensity was normalized by the following
163 equation:

164 $$I_N = \frac{I - I_b}{I_p - I_b}, \quad (1)$$

165 where I_N is the normalized brightness, I is the brightness at a particular position and time, I_b is the
166 background intensity, and I_p is the peak intensity. For **Figure 3**, I_b is the intensity at time equal 0 in the
167 center of the stencil and I_p is the peak intensity at time equal 8 h in the center of the stencil. For alginate
168 gels with no stencil and no $CaCl_2$, I_p values were from images taken of alginate gels with no stencil and
169 80 mM $CaCl_2$. For **Figure 3**, I_b is the average over the first hour between 0 and 4 mm away from the
170 center and I_p is the average intensity between 12 h and 13 h between 0 mm and 1 mm. The absolute
171 gradient is the slope of the normalized intensity as a function of radial distance (**Supplementary Figure**
172 **4**). Degradation of alginate gels was imaged the same way as described above. After 8 h of 80 mM $CaCl_2$
173 crosslinking, the solution and 5 mm diameter circle stencil were removed (t = 0 h) and the gels were
174 placed in either water, PBS, or 10% DMEM and imaged every 5 min for 8 h. Using ImageJ, the change in
175 opacity (intensity) was measured as described above at the same three locations. The intensity was
176 normalized by the following equation:

177 $$I_N = \frac{I - (I_b + \Delta I)}{I_p - (I_b + \Delta I)}, \quad (2)$$

178 where ΔI is the change in intensity due to the change in buffer added at t = 0 when either water, PBS or
179 10% DMEM is added (**Supplemental Figure 5**).

180 **2.4 Measurement of the absorbance of alginate gels during polymerization**

181 The kinetics and extent of crosslinking alginate with $CaSO_4$ and $CaCl_2$ were analyzed using a UV-Vis
182 Spectrophotometer (Varian Cary 50 Bio) and polystyrene disposable cuvettes (Semi-Micro, 1 cm path,
183 1.5 ml, 12.5 mm square x 45 mm high; Bio-Rad, 2239955). The alginate and $CaSO_4$ were mixed, and the
184 resulting 1 ml gel in the cuvette had a final concentration of 20 mg/ml alginate and 20 mM $CaSO_4$. A 1 ml
185 solution of 180 mM $CaCl_2$ or 80 mM $CaCl_2$ filled the top of the cuvette. The scans were started
186 immediately following the mixing of the alginate and $CaSO_4$ (**Supplementary Figure 2**).

187 **2.5 Elastic modulus measurement in bulk alginate gels**

188 Uniaxial compression testing was used to measure elastic modulus in bulk alginate gels. The mold was
189 removed from around the gel and a coverslip was placed on top. Compressive force was applied by
190 placing individual weights on top of the coverslip until deformation was observable. The weight was
191 incrementally increased until failure. The alginate gels were imaged 60 frames per second. (**Figure 5A**)
192 Assuming a circular cross section, the engineering stress (σ) in the gel was calculated using the following
193 equation:

194 $$\sigma = \frac{F}{A} = \frac{mg}{\frac{\pi D^2}{4}}, \quad (3)$$

195 where m is the mass of weight, g is acceleration due to gravity, A is the initial gel area and D is the
196 diameter of the top surface of the undeformed gel measured from the side view. The engineering strain (γ)
197 was calculated using the following equation:

198 $$\gamma = \frac{A_f - A_i}{A_i} \sim \frac{h_f - h_i}{h_i}, \quad (4)$$

199 where A_f and A_i are the final and initial projected trapezoid area from the side and h_f and h_i are the
200 average heights of the final and initial trapezoid shape (**Figure 5B**). Elastic modulus was calculated using
201 the following equation:

202 $$E = \frac{\sigma}{\gamma}. \quad (5)$$

203 **2.6 Functionalization of coverslips covalent attachment of alginate to coverslips**

204 Alginate gels float in both water and NaCl solutions. To prevent any movement during mechanical
205 property measurements, the alginate gels were adhered to functionalized glass coverslips[30]. First, glass
206 coverslips were submerged in piranha solution composed of 3:1 sulfuric acid (H_2SO_4, Fisher Scientific,
207 A300) and 30 wt% hydrogen peroxide (H_2O_2, Fisher Scientific, H325) for 1 h. Then the coverslips were
208 rinsed with deionized water three times before placing a solution of 1% aminoproplytriethoxysilane
209 (APTES, Acros Organics, 43094) in 0.174 M acetic acid (Fisher Scientific, A38) on top of the coverslips
210 for two hours. Afterwards the coverslips were rinsed in deionized water three times. Second, alginate was
211 attached to functionalized glass coverslips in the following way. A 1 wt% alginate solution was prepared
212 in 0.1 M 2-(N-morpholino)ethanesulfonic acid buffer (MES, Sigma Aldrich, M8250). Sulfonated N-
213 hydroxysuccinimide (NHS, Sigma Aldrich, 130672) and 1-ethyl-3-(3-dimethylaminopropyl)
214 carbodiimide (EDC, Thermo Scientific, 22980) were added to the alginate solution in a molar ratio of 1
215 alginate:30 NHS:25 EDC, and brought to a pH of 6.5 using 1 M NaOH (Fisher Scientific). To assemble
216 the functionalized alginate gels, a coverslip was placed in the bottom of the mold and 75-100 μL of the
217 functionalized alginate solution was placed on top of the functionalized coverslip so that there was a thin

218 layer of solution covering the entire surface area of the coverslip. The alginate gels were prepared as
219 described above and the initial gel was placed on top of the functionalized alginate on the coverslip.

220 **2.7 Characterization of functional attachment of alginate to glass**

221 Attenuated Total Reflectance-Fourier Transform InfraRed spectroscopy (ATR-FTIR) was performed on
222 an FTIR spectrometer (Nicolet MAGNA 750, Thermo Scientific) and attached variable-angle specular
223 reflectance accessory (Pike VeeMax III, Pike Technologies, Madison, WI, USA). ATR-FTIR was used to
224 assess whether dry, wet or unfunctionalized glass coverslips contained surface amines. In addition, the
225 density of amines on the surface of the coverslips was quantified using UV absorbance of 4-
226 nitrobenzaldehyde (4-NB, Sigma Aldrich) attached to amines on functionalized coverslips as we have
227 reported elsewhere[31]. Calibration curves of absorbance of 4-NB were generated reading spectra from a
228 UV-Vis Spectrophotometer (Varian Cary 50 Bio). To assess the degree of amine functionalization,
229 functionalized glass coverslips were immersed in a solution of 25 ml of anhydrous ethanol containing 20
230 µl of acetic acid and 0.4 mg/ml 4-nitrobenzaldehyde (4NB, Sigma Aldrich) at 50 ºC for 3 h. The
231 coverslips were then washed with absolute ethanol and dried with air and crushed and placed in a solution
232 of 0.2% acetic acid for 1 h at 30 ºC. The absorbance of 4NB was measured and the calibration curve was
233 used to calculate the number density of 4NB and consequently amines on the surface (**Supplementary**
234 **Figure 6**)[32].

235 **2.8 Measuring swelling of alginate gels**

236 Due to a difference in osmotic pressure, alginate gels swell in water. To minimize the effects of swelling
237 on the mechanical property measurements, the alginate gels were submerged in a salt solution. Alginate
238 gels were made with 20 mg/ml alginate and 20 mM $CaSO_4$. No stencils or $CaCl_2$ was used in these
239 experiments. The weight of the initial gel was measured before a sodium chloride (NaCl, Fisher
240 Scientific, S271) solution was added for 12 h. Then the salt solution was removed, and the final weight of
241 the gel was measured. The percentage swelled is calculated by dividing the mass of the water absorbed by
242 the initial mass of the gel (**Supplementary Figure 7**).

243 **2.9 Local elastic modulus measurements in alginate gels**

244 Spatial mechanical properties were measured using Atomic Force Microscopy (AFM). Functionalized
245 alginate gels were prepared as described above, and 80 mM $CaCl_2$ was placed on top of the stencil for 3
246 hours. Images were taken before and after adding and removing the 80 mM $CaCl_2$. The brightness
247 measurements from the before and after images were analyzed as described above. The gels were placed
248 into a 60 mM NaCl solution to minimize swelling for the duration of AFM testing. The force
249 measurements were performed in contact mode on a commercial AFM platform (Bio-Resolve, Bruker
250 Nano, Inc.). The AFM cantilever was 0.03 N/m. The ramp speed (i.e., force loading speed) and ramp rate

251 were 100 nm/s and 0.1 Hz, respectively. To obtain elastic modulus, E, the experimental deflection, and
252 height data was modeled by:

253 $$F = \frac{4}{3}\frac{E}{1-\nu^2}\sqrt{R\delta^3} \quad (6)$$

254 where F is the force, E is the Young's modulus (elastic modulus), ν is Poisson's ratio (0.45[33]), R is the
255 radius of spherical tip (5 μm) and δ is the indentation depth. Indentation depth is defined as the height of
256 the probe minus the deflection. To calculate the elastic modulus, the force was plotted as a function of
257 adjusted area. Adjusted area is a function of indentation depth given by:

258 $$A = \frac{4}{3}\frac{1}{1-\nu^2}\sqrt{R\delta^3} \quad (7)$$

259 The slope of the force versus adjusted area is the elastic modulus (**Supplementary Figure 8**). Three
260 locations on each gel were measured with AFM. For the circle stencil the locations were the center of the
261 stencil, 1 mm and 3 mm from the edge of the stencil. For the uniform gels without a stencil, the locations
262 were the center of the gel, and 3 mm to the left and right of the center of the gel.

263 **2.10 Collagen functionalization of alginate gels**

264 Alginate (40 mg/ml) was functionalized with EDC/NHS as described above. Collagen type I solution
265 (Cellink) was combined with 0.1 M MES buffer and 40 mM $CaSO_4$ at a pH of 6.5. Alginate gels using the
266 functionalized alginate solution and $CaSO_4$ solutions were made as described above. A 80 mM $CaCl_2$
267 solution was placed on top of the 5 mm diameter circle stencil for three hours at room temperature. Then
268 the stencil was removed, and the gels were pinned in place with a 14 mm diameter cut stencil to prevent
269 floating and movement of the gel since functionalization of glass as described above fails under
270 prolonged incubation at 37 °C. The gels were incubated in 10% DMEM for 12 h at room temperature
271 before cells and fresh media were added.

272 **2.11 Cell culture and staining**

273 MDA-MB-231 cells (human mammary carcinoma cell line, ATCC) were cultured at 37 °C with 5% CO_2
274 in DMEM with 10% heat-inactivated fetal bovine serum (FBS) (Gibco), 1% GlutaMAX (Gibco), and 1%
275 penicillin/streptomycin (Gibco). The samples were prepared with cells from subcofluent cultures (70-
276 90%) and plated at a density of 40,000-80,000 cells/cm^2. Cells were fixed with 4% paraformaldehyde
277 (Thermo Scientific) in a cytoskeleton buffer consisting of 10 mM MES (Fisher, pH 6.1), 3 mM $MgCl_2$
278 (Fisher Scientific), 138 mM KCl (Fisher Scientific), and 2 mM Ethylene Glycol Tetraacetic Acid (EGTA,
279 Sigma Aldrich). Next, cells were permeabilized using a 0.5% Triton-X cytoskeletal buffer for 5 min. For
280 staining, cells were incubated with Alexa 488-phalloidin (Thermo Fisher Scientific, A12379) in 1x Tris
281 Buffered Saline (TBS, 140 mM NaCl (Fisher Scientific) and 15 mM Tris base (Fisher Scientific), pH 7.5)
282 containing 0.1% Tween-20 (Fisher Bioreagents) v/v and 2% bovine serum albumin (Sigma Aldrich,) w/v

283 for 1 h. A circle coverslip with a diameter of 25 mm (Fisher Scientific, 1241010) was used to seal the gel
284 inside the mold. The chamber was flipped upside down for imaging with confocal microscopy.

285 **2.12 Cell imaging and analysis**

286 Live cells were imaged using a Nikon Ti-E inverted microscope with a 10x phase contrast objective (*NA*
287 = 0.3). Images of cells on the surface of the gels were taken across the diameter of the collagen
288 functionalized alginate gel. The images were stitched together using ImageJ/Fiji [34] at 4 and 24 h. The
289 total number of cells and their location relative to the edge of the stencil were recorded. After fixing and
290 staining, the cells on collagen functionalized alginate gels were imaged using a Leica Stellaris Stimulated
291 Emission Depletion (STED) confocal microscope with a 10x air objective (*NA* = 0.3). Images were taken
292 at three different locations on the gel: center, 1 mm and 3 mm from the edge of the imprinted gradient.
293 Images were taken at different depths at each location starting at the surface stepping every 10 μm into
294 the gel for a total of 21 images. The number of cells at each depth at 4 and 24 h was normalized to the
295 functionalized collagen gel at 4 or 24 h, respectively using the following equations:

296 $$N_{c,4h} = \frac{N - N_{\min}}{N_{\max,4h} - N_{\min}} \text{ and} \quad (8)$$

297 $$N_{c,24h} = \frac{N - N_{\min}}{N_{\max,24h} - N_{\min}}, \quad (9)$$

298 where N_c is the normalized number of cells at either 4 or 24 h, N is the number of cells at a particular
299 location and depth, N_{min} is the number of cells at 4 h, at the location of 3 mm from edge of stencil and at
300 depth of 200 μm inside the gel, N_{max} is the maximum number of cells at any depth within the gel and at
301 any location on the gel at 4 and 24 h, respectively.

302 **2.13 Statistical analysis**

303 The significance level is set to $p = 0.05$. Box plots: Upper and lower error bars are minimum and
304 maximum values, top and bottom of the box represent the 75th and 25th percentile, the line is the median
305 and the dashed line is the mean. The error bars shown on the figures are 95% confidence intervals. *T*-tests
306 were used to gauge statistical significance of mechanical property difference and statistical significance
307 was set at $p = 0.05$ and denoted with an asterisk.

3. Results:

3.1 Unique stencil patterns result in tunable opacity patterns

Gradients in alginate crosslinking were generated leveraging diffusion of calcium through custom designed stencils. Alginate (20 mg/ml) sparsely crosslinked with calcium sulfate (20 mM $CaSO_4$) was loaded into molds with a recessed shelf (**Figure 1A**). This shelf allows for the application of a clear stencil on top of the gel. The stencil contains a customizable pattern cut into cellulose acetate using a craft cutter (**Figure 1B**). This particular craft cutter is able to cut sizes as small as 1 mm (**Supplementary Figure 1**). A high concentration calcium chloride solution (80 mM $CaCl_2$) was placed on top of the stencil. Calcium diffuses into the gel through the pattern, creating a gradient in opacity in the *x-y* plane (**Figure 1C**). The opacity was quantified by calculating the intensity of the alginate gel at a particular position and time. Opacity is highest underneath the pattern and increased with time. In addition to opacity gradient formation in thick alginate gels in molds, opacity gradients also formed in thin alginate gels (2 mm) fabricated in silicone wells cut to different shapes (**Figure 2A**). Thin multilayer chambers with both unique well patterns and unique stencils were assembled in petri dishes. Sparsely crosslinked alginate was loaded into these thin wells, overlaid with a stencil and submerged in high concentration calcium chloride (**Figure 2B**). This resulted in increased intensity over a period of 8 h, producing a gradient in intensity templated by the stencil pattern (**Figure 2C**). This demonstrates that opacity gradients can be imprinted into either thick or thin gels by tuning the stencil pattern and duration of gradient development, allowing for a tremendous amount of flexibility in creating opacity gradients with different shapes and gradient steepness.

3.2 Characterization of opacity gradients and kinetics of change in opacity

Given that unique gradients can be formed using different stencil patterns, the kinetics of spatial pattern formation was assessed using both absorbance of alginate gels within cuvettes and intensity of alginate gels imaged within the molds over time. Intensity from images at different positions and at different times was normalized to the maximum intensity within the alginate gel. Alginate gels sparsely crosslinked with two different concentrations of calcium sulfate and exposed to different concentrations of calcium chloride showed that above 50 mM $CaCl_2$ a maximum level of absorbance was attained, indicating that the high concentration calcium chloride solution (80 mM $CaCl_2$) used above was saturating, so this concentration was selected for further experiments (**Supplementary Figure 2A**). Four different stencil model patterns were used (**Figure 3A**). Sparsely crosslinked alginate gels exposed to high concentrations of calcium chloride without a stencil produced a high intensity alginate gel with no gradient (**Figure 3B**). The contraction of the alginate gel upon crosslinking is revealed by the thin black crescent formed when the gel pulled away from the mold. Alginate gels exposed to water instead of calcium chloride resulted in a gel with no change in intensity within the gel. To characterize the spatial kinetics of intensity changes,

342 the normalized intensity of these gels was calculated at the center and at 1 and 3 mm away from the edge
343 of the stencil between 0 and 8 h (**Figure 3C**). The alginate gels exposed to calcium chloride with no
344 stencil had the same rate of increase in intensity at all three locations. After 2 h, the intensity within the
345 alginate gels reached its maximum and remained constant for the remaining 8 h. Similar kinetics were
346 observed when measuring the absorbance within cuvettes of the sparsely crosslinked alginate gels
347 exposed overtop to high concentrations of calcium chloride (**Supplementary Figure 2B**). Interestingly,
348 two behaviors were observed in the cuvette absorbance experiments, one that matched the kinetics of the
349 imaging in **Figure 3C** and one that was much slower. The slow increase in absorbance is consistent with
350 a moving front of opacity oriented in the downward position of the cuvette, while the fast increase is
351 consistent with a moving front of opacity oriented from the sides of the cuvette. Alginate gels contract
352 after crosslinking, resulting in an occasional pulling away from the sides of the cuvette, creating a channel
353 along the side that filled with high concentration calcium chloride. Indeed, a simple diffusion rate
354 calculation based on the diffusion coefficient of calcium (1300 $\mu m^2/s$) and different length scales (height
355 = 3 mm vs half-width = 1 mm) for the two scenarios predicts a lag of 1-2 h as compared to the fast
356 kinetics. This is precisely what is observed (**Supplementary Figure 2B**). Finally, the alginate gels that
357 were not exposed to $CaCl_2$ produce no change in intensity at any of the locations (**Figure 3C**). These data
358 indicate that alginate gels crosslink over 2 h before coming to a steady-state level.
359 In addition to the no stencil condition, the spatial kinetics of different stencil patterns were
360 quantified. Sparsely crosslinked alginate gels were exposed to high calcium chloride solutions through the
361 circle, line and S stencil (**Figure 3B**) and intensity was measured at the center as well as 1 and 3 mm
362 away from the edge of the stencil (**Figure 3D-F**). The opacity pattern matched the shape of the stencil
363 (**Figure 3B**). In addition to water, alginate gels were assembled in a common buffer (PBS) and cell
364 culture media (DMEM). Intensity gradients formed in these buffers but these gradients were shallower
365 (**Supplementary Figure 3**). For all stencils as the distance from the center of the stencil increases, the
366 increase in intensity over time is slower. The center location, where the gel is directly exposed to the
367 calcium chloride on every stencil increases in intensity with similar kinetics to the no stencil condition.
368 The lag time associated with increases in intensity 3 mm from the stencil edge varied among the stencil
369 shape with the circle stencil being the longest, followed by the line and S stencil (**Figure 3D-F**). The
370 slower kinetics associated with the line stencil as compared to the S stencil is caused by the thinner width
371 of the line stencil compared to the S stencil **(Figure 3E&F**). Quantifying the intensity kinetics for
372 different stencil shapes allow for the selection of a particular time that results in a specific opacity
373 gradient.
374 Given that the line and S stencil shapes had different widths and resulted in different intensity
375 kinetics far from the center, the effect of the size of the stencil for one particular shape was assessed.

376 Circle stencils with diameters of 5 and 2.5 mm were used to form radial gradients (**Figure 4**). Radial
377 gradients were quantified by averaging linescans over angles between 0 and 2π and absolute gradient was
378 quantified by finding the local slope of the radial profile at each point (**Supplementary Figure 4**). The
379 circle stencils showed the characteristic decrease in intensity further from the stencil. Interestingly, these
380 gradients seemed stable, even when the calcium chloride solution was removed and replaced with water
381 (**Supplementary Figure 5**). Large circle stencils showed an increase in intensity far from the stencil for
382 long periods, suggesting the impact of a no flux boundary condition at the outer edge of the mold (**Figure**
383 **4A**). This effect was diminished with the smaller circle stencil, indicating that the domain in which
384 diffusion is occurring is essentially semi-infinite for times less than 16 h (**Figure 4B**). Using a simple
385 point source model, the diffusion coefficient in the alginate gel was predicted to be on the order of 160
386 $\mu m^2/s$, which is about 8-fold lower than that in water, likely slowed by the binding of calcium to alginate.
387 Absolute gradients were calculated for both large and small stencil over time, requiring about 4 h for
388 significant gradient establishment. Gradient steepness increased over time and similar gradients occurred
389 in both small and large circle stencils. Large circle stencils produce robust opacity gradients after 4 h near
390 the stencil edge, but these opacity gradients dramatically flatten far from the stencil. Small circle stencils
391 on the other hand can be treated as semi-infinite point sources that produces robust opacity gradients after
392 4 h throughout the gel.

393 **3.3 Characterization of bulk mechanical properties of alginate gels**

394 Given the effects of alginate gel crosslinking on opacity characterized above, we are were interested in
395 measuring the bulk mechanical properties of the alginate gels under similar crosslinking conditions. We
396 used compression testing to assess the compressive elastic modulus of alginate gels. Different masses
397 were placed on top of the alginate gel and the deformation of the alginate was quantified from images
398 (**Figure 5A**). The slope of the stress versus strain curve equals the elastic modulus of the gel (**Figure 5B**).
399 Alginate gels (20 mg/ml) were sparsely crosslinked with different calcium sulfate concentrations (10 mM,
400 20 mM or 40 mM) in the absence of stencils. The elastic modulus of the alginate gels increased slightly
401 with the concentration of $CaSO_4$ (**Figure 5C**). Under conditions used above, the median compressive
402 elastic modulus of the sparsely crosslinked gel is ~1.5 kPa. When these gels are exposed to high
403 concentrations of calcium chloride, the compressive elastic modulus increased 16-fold (**Figure 5D**). This
404 indicates that alginate gels crosslinked in the stencil system above span roughly 1.5-25 kPa.

405 **3.4 Spatial patterns of stiffness can be imprinted into alginate gels**

406 Given the ability to control spatial alginate gel crosslinking using stencils and that this crosslinking results
407 in increases in elastic modulus, we wondered if gradients of elastic modulus were formed and if opacity
408 was predictive of elastic modulus. The elastic modulus was determined at various positions on alginate
409 gels before and after crosslinking with high concentration calcium chloride using AFM. In order to secure

410 the alginate gel to the glass surface, we used EDC/NHS chemistry to attach a layer of alginate to amine
411 functionalized glass. This layer of alginate attaches to the crosslinked alginate gel that was placed over
412 top. This attachment is robust at room temperature, but the attachment is weak if the gel is heated to 37
413 ºC. We verified glass functionalization by identifying both C-N and $–NH_2$ bonds formed after aminosilane
414 chemistry (**Supplementary Figure 6A**). An amine-containing molecule absorbing at around 270 nm (4-
415 nitrobenzyaldeyde (4NB)) was coupled to the functionalized surface, washed, released after hydrolysis
416 and absorbance was measured at 270 nm in order to determine the amine density. Using a calibration
417 curve for 4NB, we determined that the number density of amines to be about 10^7 #/μm^2 (**Supplementary**
418 **Figure 6B-D**). This resulted in alginate gels attached to the glass surface. Indeed, the radial contraction of
419 the alginate gel that is normally observed is not observed when the gel is attached to the glass surface
420 (**Supplementary Figure 6E**). To limit swelling of the alginate gels, gels were submersed in a sodium
421 chloride solution (60 mM NaCl), allowing for AFM measurements to be done in solution
422 (**Supplementary Figure 7**). Using AFM, a spherical probe attached to a cantilever was brought in contact
423 with the alginate gels and the height and deflection of the cantilever was measured (**Supplementary**
424 **Figure 8**). This allowed for the measurement of elastic modulus in solution at multiple positions.
425 First, sparsely crosslinked alginate gels were exposed to a high concentration calcium chloride.
426 Images were taken before and after crosslinking (**Figure 6A**). The characteristic increase in opacity after
427 crosslinking was observed. The elastic modulus was calculated at the center of the gel and 3 mm to the
428 right and left of the center of the gel, yielding similar values (~40 kPa). There was not a statistical
429 difference in opacity at those three points. Second, sparsely crosslinked alginate gels were exposed to a
430 high concentration calcium chloride solution through a large (5 mm) circle stencil (**Figure 6B**). This
431 yielded a radial gradient in opacity. The elastic modulus was calculated at the center of the gel and 1 and
432 3 mm to the right edge of the stencil. In the center of the gel, the elastic modulus was high (30 kPa), but
433 further away the elastic modulus was much lower (~10 kPa). These gels showed larger changes in
434 opacity. Finally, sparsely crosslinked alginate gels were exposed to 60 mM NaCl (**Figure 6C**). This
435 yielded no increase in opacity. The elastic modulus was calculated at the center of the gel and 3 mm to the
436 right and left of the center of the gel, yielding similar values (~1.5 kPa). All points both before and after
437 addition of the 60 mM NaCl showed no visible difference in opacity. This demonstrates that elastic
438 modulus differs spatially across gradients formed using stencils and that there is likely a relationship
439 between opacity and elastic modulus.
440 Given that both the elastic modulus and intensity decrease as a function of distance from the edge
441 of the stencil, we overlaid elastic modulus and normalized intensity (**Figure 7A**). Similar decreases are
442 observed for both opacity and elastic modulus. When the elastic modulus for each measurement is plotted
443 against the corresponding normalized intensity, the result is a sigmoidal curve where the intensity

444 increases with elastic modulus (**Figure 7B**). The half max for the sigmoidal fit is 8 kPa, indicating a steep
445 increase in opacity. It appears that while opacity indicates stiffness changes, this range only spans from 5
446 kPa to 15 kPa.

447 **3.5 Cell invasion into the alginate gel is stiffness dependent**

448 After establishing that gradients in mechanical properties can be generated using this stenciling approach,
449 cellular responses to these gradients were investigated. Alginate is weakly cell adhesive so the alginate
450 was functionalized with collagen and then weakly crosslinked using the $CaSO_4$ solution. A 5 mm
451 diameter stencil and 80 mM $CaCl_2$ was used to imprint a radial gradient in the center of the alginate gel.
452 Overlapping images across the diameter of the collagen functionalized alginate gel were taken of breast
453 cancer cells (MDA-MB-231) on the surface of the gel and stitched together (**Figure 8A**). When alginate
454 was not functionalized with collagen, there were fewer cells on the surface at 4 h compared to the
455 collagen functionalized alginate gels (**Figure 8B**). Interestingly after 24 h the number of cells on the
456 surface of the collagen gels significantly decreased. The decrease in cell number could either be due to
457 cell death or cell invasion. Consequently, we fixed and stained cells for F-actin at 4 and 24 h and used
458 confocal microscopy to image cells at different positions corresponding to different stiffnesses previously
459 assessed by AFM (**Figure 8C**). Images were taken at different depths at these three spatial positions.
460 Cells are seen in the center of collagen functionalized alginate gels at the surface at 4 h. However, they
461 are no longer present at 24 h at the same position (**Figure 8D**). Conversely, cells are not seen in the center
462 of the collagen functionalized alginate gel 150 μm under the surface at 4 h. However, they are observed at
463 that depth at 24 h, indicating invasion. We quantified the cell density at different depths (**Figure 8F**).
464 Very little cell attachment is shown in the absence of collagen. However, there is a robust decrease in cell
465 density as a function of depth for all three positions at 4 h on collagen functionalized alginate gels. In the
466 center, where the stiffness is higher, there is more robust invasion of cells into the collagen functionalized
467 alginate gel resulting in both a decrease in cell number at the surface and an increase in cell number at
468 lower depths at 24 h. There is approximately similar invasion at 1 mm from the stencil edge, however,
469 more cells remain closer to the surface. Interestingly, there is very little cell invasion at 3 mm from the
470 stencil edge, resulting in a depth dependent cell density that is roughly similar between 4 and 24 h. This
471 demonstrates that imprinting of mechanical property gradients using this unique approach can create
472 spatially dependent invasion patterns in breast cancer cells.

4. Discussion:

In this paper we created an approach to generate tunable and reproducible gradients in both thick and thin alginate gels using an easy stenciling approach. We characterized the crosslinking kinetics a number of different ways and showed that geometry and gradient development time can tune both the average opacity and opacity gradient steepness in known and reproducible ways. We measured Young's modulus in both bulk materials as well as spatially, demonstrating that the opacity gradient mapped to the stiffness gradient and quantified the range of stiffness over which opacity was a good proxy for stiffness. We demonstrate a method of functionalizing stiffness gradient alginate with collagen resulting in spatially dependent cell invasion into the alginate gel.

Opacity changes in alginate have been observed previously. However, the mechanism for changes in opacity are obscure. Opacity changes are likely due to increases in light scattering caused by local contraction and densification of the alginate network. This is likely, given that hydrogel opacity varies with polymer molecular weight, concentration and crosslinking density and high water content hydrogels have refractive indices similar to that of water[35]. Gel contraction is likely driven by minimizing free energy due to the decrease in entropy associated with the crosslinks[36]. Interestingly, we observed flow from outer edges in areas that were not opaque towards the opaque center when using radial stencils. This flow pattern changes based on the shape of the stencil. This directed contraction could be leveraged as a way to locally stimulate cells by inducing shear or compressive stresses upon the cells. In addition, interpenetrating networks composed of alginate and fiber forming polymers like collagen or fibrin could be assembled. The spatially controlled contraction that occurs within these alginate gels could be used to align or structure the fiber network in these composite networks. Consequently, the contraction may be leveraged in interesting ways. Applications that require either cell embedding or assembly of the gradient on tissue will need to account for this contraction and if undesired, approaches to mitigate it by using a stiffer initial gel or altering ionic strength of the crosslinking gel could be used.

As a demonstration of the utility of these gradients we examined cancer cell invasion into these alginate gradient gels. We showed spatial control over invasion through the stiffness gradient formation. Cancer cells in regions that were stiffer invaded more efficiently than in regions that were softer. This broadly agrees with what has been seen in other systems examining the role of stiffness in controlling cell migration and invasion[37]. Others have shown invasion into alginate gels that is stiffness dependent although under certain circumstances higher stiffness either stunts migration or facilitates it [38–40]. This seems to be dependent on the extracellular matrix additions to the alginate including fibrillar collagen or decellularized extracellular matrix. More recently, the plastic nature of the extracellular matrix has become an appreciated mechanical modulator of cancer cell migration to complement the already established role for elastic behavior in driving cancer invasion[41]. Future efforts focusing on controlling

viscoelastic properties spatially using this technique will likely uncover novel roles for the spatial regulation of cell behavior through plastic deformations of the extracellular matrix.

One potential use for these gradient gels would be in experiments exploring fundamental aspects of durotaxis. While there are many examples of creating 2D stiffness gradients to explore how signaling or the cytoskeleton regulates durotaxis, there are many fewer examples of mechanistic studies of durotaxis in 3D. The Young's modulus probed in this work (0.5-50 kPa) and in particular the Young's modulus over which opacity is a good proxy for stiffness (5-15 kPa) matches well with other work characterizing Young's modulus in alginate gels[42–44] and overlaps nicely with soft tissues and the range of mechanosensitivity of many types of cells[45]. Alginate is a relatively inert molecule and many cells do not attach to it. However, by functionalizing the alginate gel with collagen, cells can invade the gel, allowing for studies of durotaxis in 3D. Consequently, there is an opportunity to attach extracellular matrix molecules to the alginate to study durotaxis across a variety of ligand-receptor pairs. Furthermore, there are opportunities to assemble interpenetrating networks composed of both alginate and collagen and create similar gradients, assessing whether cells can sense stiffness gradients in alginate through the collagen network[44,46]. After stiffness gradient imprinting, different stencils could be used to generate similar or spatially distinct gradients of soluble factor to explore how cells integrate durotactic and chemotactic cues. Collagen fibers within the networks could be aligned using magnetic fields[47,48] or local mechanical rotation[49], allowing to probe competition or cooperation between contact guidance and durotaxis. Understanding how different cells integrate these signals and leverage overlapping or distinct intracellular signaling networks is an understudied area and is absolutely critical for the assembly of complex tissues.

Another potential use for this system would be as an advanced wound dressing. There are other examples of systems that have used soluble gradients to direct cell migration in the hope of enhancing wound healing[50,51]. However, to our knowledge there are no reports of efforts using stiffness gradients to enhance wound healing, even though stiffness gradients are features of healing wounds[14]. As mentioned above, alginate has already been used as a wound dressing, but mainly for its ability to absorb exudate. Either attaching extracellular matrix or assembling an interpenetrating network would allow for its use as a provisional matrix, guiding cell movement into the provisional matrix through gradients of stiffness. The versatility of this technique could be leveraged to generate gradients that best match the geometry and mechanics of the wound. The ease in creating these gradients will allow non-experts the ability to create made-to-order wound dressings.

5. Conclusions:

Stencils can be used to generate gradients in opacity within alginate gels. These stencils can be easily designed and fabricated using a common craft cutter. Different stencil shapes result in different gradients in opacity that can be imprinted into both thick and thin alginate gels of arbitrary shape. The steepness of the opacity gradient as well as the maximum opacity can be controlled based on reproducible crosslinking kinetics regulated through calcium concentration and gradient developing time. Calcium crosslinking results in both opacity changes as well as increases in elastic modulus in the bulk hydrogel. Spatial gradients in elastic modulus can also be imprinted into alginate gels using this stenciling approach. Opacity correlates with elastic modulus, allowing it to be used as a proxy for local elastic modulus. Finally, gradient alginate gels can be functionalized with collagen facilitating cancer cell invasion that occurs at different rates depending on the spatial position of the cell.

Acknowledgements:

We acknowledge Megan Wolfe, Sarah Fangrow, Maria Lebedeva, Madison Karamagianis, Flora Kafunda, Clarissa Carolan, Claire Allen from the Freshman Honors Research Program. We also acknowledge Margie Carter and the Office of Biotechnology and the Roy J. Carver High Resolution Microscopy Facility for help with the confocal microscopy.

555 **References:**

556 [1] Shellard A and Mayor R 2021 Collective durotaxis along a self-generated stiffness gradient in vivo
557 *Nature* **600** 690–4

558 [2] Janssen E, van den Dries K, Ventre M and Cambi A 2024 Mechanobiology of myeloid cells
559 *Current Opinion in Cell Biology* **86** 102311

560 [3] Harn H I-C, Ogawa R, Hsu C-K, Hughes M W, Tang M-J and Chuong C-M 2019 The tension
561 biology of wound healing *Experimental Dermatology* **28** 464–71

562 [4] Ayad N M E, Kaushik S and Weaver V M 2019 Tissue mechanics, an important regulator of
563 development and disease *Philosophical Transactions of the Royal Society B: Biological Sciences*
564 **374** 20180215

565 [5] Tschumperlin D J and Lagares D 2020 Mechano-therapeutics: Targeting Mechanical Signaling in
566 Fibrosis and Tumor Stroma *Pharmacology & Therapeutics* **212** 107575

567 [6] Kloxin A M, Benton J A and Anseth K S 2010 In situ elasticity modulation with dynamic
568 substrates to direct cell phenotype *Biomaterials* **31** 1–8

569 [7] Zhu D, Trinh P, Li J, Grant G A and Yang F 2021 Gradient hydrogels for screening stiffness effects
570 on patient-derived glioblastoma xenograft cellfates in 3D *J Biomed Mater Res A* **109** 1027–35

571 [8] Auxillos J, Crouigneau R, Li Y-F, Dai Y, Stigliani A, Tavernaro I, Resch-Genger U, Sandelin A,
572 Marie R and Pedersen S F 2024 Spatially resolved analysis of microenvironmental gradient impact
573 on cancer cell phenotypes *Science Advances* **10** eadn3448

574 [9] Tong X, Jiang J, Zhu D and Yang F 2016 Hydrogels with Dual Gradients of Mechanical and
575 Biochemical Cues for Deciphering Cell-Niche Interactions *ACS Biomaterials Science and*
576 *Engineering* **2** 845–52

577 [10] Hadden W J, Young J L, Holle A W, McFetridge M L, Kim D Y, Wijesinghe P, Taylor-Weiner H,
578 Wen J H, Lee A R, Bieback K, Vo B-N, Sampson D D, Kennedy B F, Spatz J P, Engler A J and
579 Choi Y S 2017 Stem cell migration and mechanotransduction on linear stiffness gradient hydrogels
580 *Proceedings of the National Academy of Sciences* **114** 5647–52

581 [11] DuChez B J, Doyle A D, Dimitriadis E K and Yamada K M 2019 Durotaxis by Human Cancer
582 Cells *Biophysical Journal* **116** 670–83

583 [12] Hakeem R M, Subramanian B C, Hockenberry M A, King Z T, Butler M T, Legant W R and Bear J
584 E 2023 A Photopolymerized Hydrogel System with Dual Stiffness Gradients Reveals Distinct
585 Actomyosin-Based Mechano-Responses in Fibroblast Durotaxis *ACS Nano* **17** 197–211

586 [13] Sunyer R, Conte V, Escribano J, Elosegui-Artola A, Labernadie A, Valon L, Navajas D, García-
587 Aznar J M, Muñoz J J, Roca-Cusachs P and Trepat X 2016 Collective cell durotaxis emerges from
588 long-range intercellular force transmission *Science* **353** 1157–61

589 [14] Harn H I-C, Chiu P-Y, Lin C-H, Chen H-Y, Lai Y-C, Yang F-S, Wu C-C, Tang M-J, Chuong C-M
590 and Hughes M W 2022 Topological Distribution of Wound Stiffness Modulates Wound-Induced
591 Hair Follicle Neogenesis *Pharmaceutics* **14** 1926

592 [15] Liang Y, He J and Guo B 2021 Functional Hydrogels as Wound Dressing to Enhance Wound
593 Healing *ACS Nano* **15** 12687–722

594 [16] Aderibigbe B A and Buyana B 2018 Alginate in Wound Dressings *Pharmaceutics* **10** 42

595 [17] Lee K Y and Mooney D J 2012 Alginate: Properties and biomedical applications *Progress in*
596 *Polymer Science (Oxford)* **37** 106–26

597 [18] Pebworth M-P, Cismas S A and Asuri P 2014 A Novel 2.5D Culture Platform to Investigate the
598 Role of Stiffness Gradients on Adhesion-Independent Cell Migration *PLOS ONE* **9** e110453

599 [19] Tabriz A G, Hermida M A, Leslie N R and Shu W 2015 Three-dimensional bioprinting of complex
600 cell laden alginate hydrogel structures *Biofabrication* **7** 045012

601 [20] Sardelli L, Pacheco D, Zorzetto L, Rinoldi C, Święszkowski W and Petrini P 2019 Engineering
602 biological gradients *Journal of Applied Biomaterials & Functional Materials* **17**
603 2280800019829023

604 [21] Engler J.R. A J and T and Engler J.R. A J and T 2010 Preparation of Hydrogel Substrates with
605 tunable Mechanical Properties *Current Protocols in Cell Biology* **Unit 10.16** 10.16.1-10.16.16

606 [22] Sundararaghavan H G, Monteiro G A, Firestein B L and Shreiber D I 2009 Neurite growth in 3D
607 collagen gels with gradients of mechanical properties *Biotechnology and Bioengineering* **102** 632–
608 43

609 [23] Bouzos E and Asuri P 2023 Sandwich Culture Platforms to Investigate the Roles of Stiffness
610 Gradients and Cell–Matrix Adhesions in Cancer Cell Migration *Cancers* **15** 1729

611 [24] Silva J M, Caridade S G, Oliveira N M, Reis R L and Mano J F 2015 Chitosan–alginate
612 multilayered films with gradients of physicochemical cues *J. Mater. Chem. B* **3** 4555–68

613 [25] Erickson A E, Sun J, Lan Levengood S K, Swanson S, Chang F-C, Tsao C T and Zhang M 2019
614 Chitosan-based composite bilayer scaffold as an in vitro osteochondral defect regeneration model
615 *Biomed Microdevices* **21** 34

616 [26] Zhang Y, Xue Y, Ogawa T, Wada S and Wang J-Y 2023 3D Printed Alginate Hydrogels with
617 Stiffness-Gradient Structure in a Carbomer Supporting Bath by Controlled Ca2+ Diffusion *ACS*
618 *Appl. Eng. Mater.* **1** 802–12

619 [27] Ma Y, Wang Y, Chen D, Su T, Chang Q, Huang W and Lu F 2023 3D bioprinting of a gradient
620 stiffened gelatin–alginate hydrogel with adipose-derived stem cells for full-thickness skin
621 regeneration *J. Mater. Chem. B* **11** 2989–3000

622 [28] Wang Y, Zhang J, Shu X, Wu F and He J 2024 Controlled domain gels with a wide stiffness
623 gradient simultaneously promote bone regeneration and suppress tumor recurrence through DAPK
624 activity *Chemical Engineering Journal* **482** 149018

625 [29] Stowers R S, Allen S C and Suggs L J 2015 Dynamic phototuning of 3D hydrogel stiffness
626 *Proceedings of the National Academy of Sciences* **112** 1953–8

627 [30] Cha C, Antoniadou E, Lee M, Jeong J H, Ahmed W W, Saif T A, Boppart S A and Kong H 2013
628 Tailoring Hydrogel Adhesion to Polydimethylsiloxane Substrates Using Polysaccharide Glue
629 *Angewandte Chemie International Edition* **52** 6949–52

630 [31] Unnikandam Veettil S R S R, Van Bruggen S M S M, Hwang D-G D G, Bartlett M D M D and
631 Schneider I C I C 2019 Tuning surface functionalization and collagen gel thickness to regulate
632 cancer cell migration *Colloids and Surfaces B: Biointerfaces* **179** 37–47

633 [32] Xiang S, Xing G, Xue W, Lu C and Lin J-M 2012 Comparison of two different deposition methods
634 of 3-aminopropyltriethoxysilane on glass slides and their application in the ThinPrep cytologic test
635 *Analyst* **137** 1669–73

636 [33] Caliari S R and Burdick J A 2016 A Practical Guide to Hydrogels for Cell Culture *Nat Methods* **13**
637 405–14

638 [34] Preibisch S, Saalfeld S and Tomancak P 2009 Globally optimal stitching of tiled 3D microscopic
639 image acquisitions *Bioinformatics* **25** 1463–5

640 [35] Martin-Saldaña S, Al Waeel M, Alsharabasy A M, Daly A and Pandit A 2022 An interdisciplinary
641 framework for the characterization of extracellular matrix-hydrogels for biomedical applications
642 *Matter* **5** 3659–705

643 [36] Łabowska M B, Jankowska A M, Michalak I and Detyna J 2021 Shrinkage of Alginate Hydrogel
644 Bioinks Potentially Used in 3D Bioprinting Technology *Key Engineering Materials* **885** 39–45

645 [37] Oudin M J and Weaver V M 2016 Physical and Chemical Gradients in the Tumor
646 Microenvironment Regulate Tumor Cell Invasion, Migration, and Metastasis *Cold Spring Harb*
647 *Symp Quant Biol* **81** 189–205

648 [38] Liu C, Lewin Mejia D, Chiang B, Luker K E and Luker G D 2018 Hybrid collagen alginate
649 hydrogel as a platform for 3D tumor spheroid invasion *Acta Biomaterialia* **75** 213–25

650 [39] Chang J, Pang E M, Adebowale K, Wisdom K M and Chaudhuri O 2020 Increased Stiffness
651 Inhibits Invadopodia Formation and Cell Migration in 3D *Biophysical Journal* **119** 726–36

652 [40] Cai G, Li X, Lin S-S, Chen S J, Rodgers N C, Koning K M, Bi D and Liu A P 2024 Matrix
653 confinement modulates 3D spheroid sorting and burst-like collective migration *Acta Biomaterialia*
654 **179** 192–206

655 [41] Wisdom K M, Adebowale K, Chang J, Lee J Y, Nam S, Desai R, Rossen N S, Rafat M, West R B,
656 Hodgson L and Chaudhuri O 2018 Matrix mechanical plasticity regulates cancer cell migration
657 through confining microenvironments *Nat Commun* **9** 4144

658 [42] Chaudhuri O, Gu L, Klumpers D, Darnell M, Bencherif S A, Weaver J C, Huebsch N, Lee H,
659 Lippens E, Duda G N and Mooney D J 2016 Hydrogels with tunable stress relaxation regulate stem
660 cell fate and activity *Nature Mater* **15** 326–34

661 [43] Freeman F E and Kelly D J 2017 Tuning Alginate Bioink Stiffness and Composition for Controlled
662 Growth Factor Delivery and to Spatially Direct MSC Fate within Bioprinted Tissues *Sci Rep* **7**
663 17042

[44] da Cunha C B, Klumpers D D, Li W A, Koshy S T, Weaver J C, Chaudhuri O, Granja P L and Mooney D J 2014 Influence of the stiffness of three-dimensional alginate/collagen-I interpenetrating networks on fibroblast biology *Biomaterials* **35** 8927–36

[45] Discher D E, Smith L, Cho S, Colasurdo M, García A J and Safran S 2017 MATRIX MECHANOSENSING: From Scaling Concepts in 'Omics Data to Mechanisms in the Nucleus, Regeneration, and Cancer *Annu Rev Biophys* **46** 295–315

[46] Munoz-Pinto D J, Jimenez-Vergara A C, Gharat T P and Hahn M S 2015 Characterization of sequential collagen-poly(ethylene glycol) diacrylate interpenetrating networks and initial assessment of their potential for vascular tissue engineering *Biomaterials* **40** 32–42

[47] Tranquillo R T, Girton T S, Bromberek B A, Triebes T G and Mooradian D L 1996 Magnetically orientated tissue-equivalent tubes: Application to a circumferentially orientated media-equivalent *Biomaterials* **17** 349–57

[48] Guo C and Kaufman L J 2007 Flow and magnetic field induced collagen alignment *Biomaterials* **28** 1105–14

[49] Nuhn J A M, Perez A M and Schneider I C 2018 Contact guidance diversity in rotationally aligned collagen matrices *Acta Biomaterialia* **66** 248–57

[50] Xu Z, Wu J, Gong P and Chang C 2023 Accelerate wound healing by microscale gel array patch encapsulating defined SDF-1α gradient *Journal of Controlled Release* **358** 1–12

[51] Rahmati M, Blaker J J, Lyngstadaas S P, Mano J F and Haugen H J 2020 Designing multigradient biomaterials for skin regeneration *Materials Today Advances* **5** 100051

Sources of Support:

This work was supported by the Freshman Honors Research Program at Iowa State University, the Griswold Internship Program, the National Science Foundation under grant No. EEC 1852125 and the National Institutes of Health under grant No. GM143302.

Data Availability:

Author Contributions:

Z.O.: Conceived, conducted, analyzed the experiments and interpreted the data across figures 1, 3, 6-8, S1 and S5-S8, wrote the article, prepared the figures and edited the article. T.P.: Conceived, conducted, analyzed the experiments and interpreted the data across figures 4, 5 and S4, wrote the article, prepared the figures and edited the article. J.Z.: Conceived, conducted, analyzed the experiments and interpreted the data across figures 6 and S8, wrote the article and edited the article. A.F.: Conceived and conducted experiments and interpreted the data in figure 8, wrote the article and edited the article. F.R.N.: Conceived and conducted experiments in figure 8, wrote the article and edited the article. T.K.: Conceived the experiments in figures 1 and 3 and edited the article. N.J.: Conceived, conducted, analyzed the experiments and interpreted the data in figure 2. T.G.: Conceived, conducted, analyzed the experiments and interpreted the data in figure S3. M.T.: Conceived, conducted, analyzed the experiments and interpreted the data in figure S2, wrote the article and edited the article. E.M.: Conceived and printed molds used across all figures, wrote the article and edited the article. L.M.: Conducted the experiments in Figure S6. A.K.: Conducted the experiments in Figure S6. A.M.: Conceived molds used across all figures and edited the article. J.R.: Conceived and interpreted the data across figures 6 and S8. I.C.S.: Conceived, analyzed the data and interpreted the data across all figures, wrote the article, prepared the figures and edited the article.

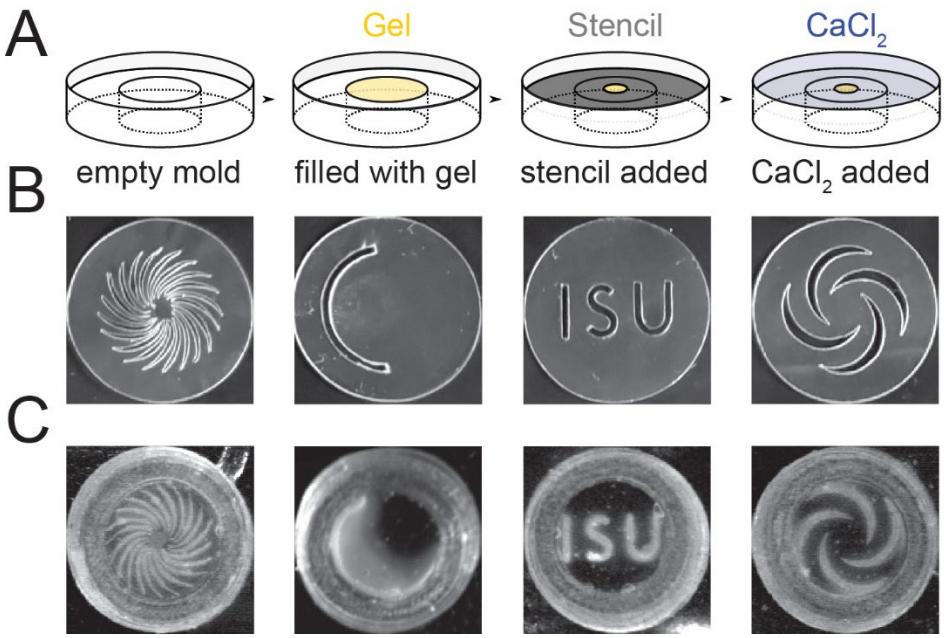

Figure 1: Approach for stenciling opacity gradients into alginate gels. A) Schematic of approach to fabricate alginate gels. Alginate gels (2700 - 5400 μm thick) are initially sparsely cross-linked using low calcium concentration (20 mM $CaSO_4$) in molds (yellow). A stencil is placed above with different geometries of openings (grey). A solution of high calcium concentration (80 mM $CaCl_2$) is placed on top of the stencil to spatially cross-link the gel (blue). B) Images of uniquely designed stencils made of transparency film (cellulose acetate, 10 μm thick) cut using a craft cutter. C) Images of alginate hydrogels spatially cross-linked using stencils in B) after > 1h 20 min of incubation. Images are 25.4 mm by 25.4 mm.

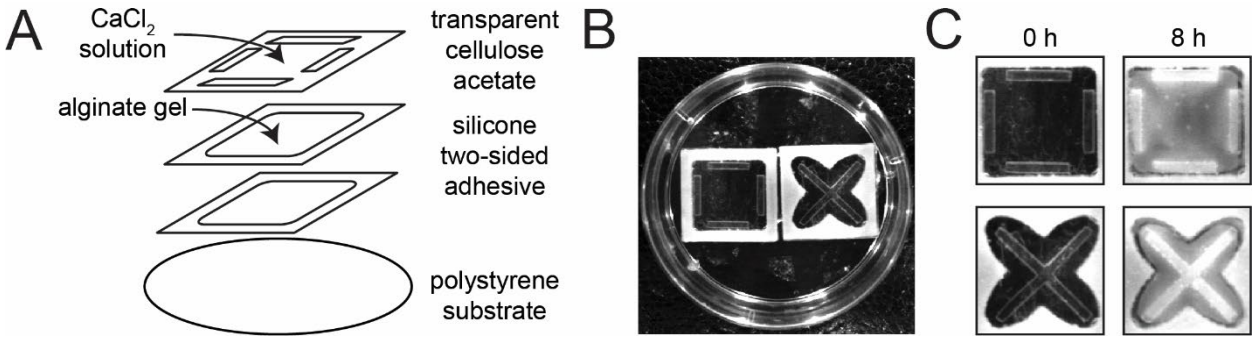

Figure 2: Stencils can generate opacity gradients in thin alginate gels. A) Two–sided adhesive silicone sheets cut with patterns were doubly stacked creating a 2 mm thick reservoir to hold sparsely cross-linked alginate gels (20 mg/ml alginate gelled with 20 mM $CaSO_4$). This reservoir was adhered to a polystyrene cell culture dish. A stencil was adhered to the top silicone sheet and the cell culture dish was filled with 80 mM $CaCl_2$ to crosslink alginate gel exposed to the solution. B) Image of two chambers attached to one 35 mm polystyrene cell culture dish. The silicone well is white. C) Images were taken before crosslinking (0 h) and after crosslinking (8 h) with 80 mM $CaCl_2$.

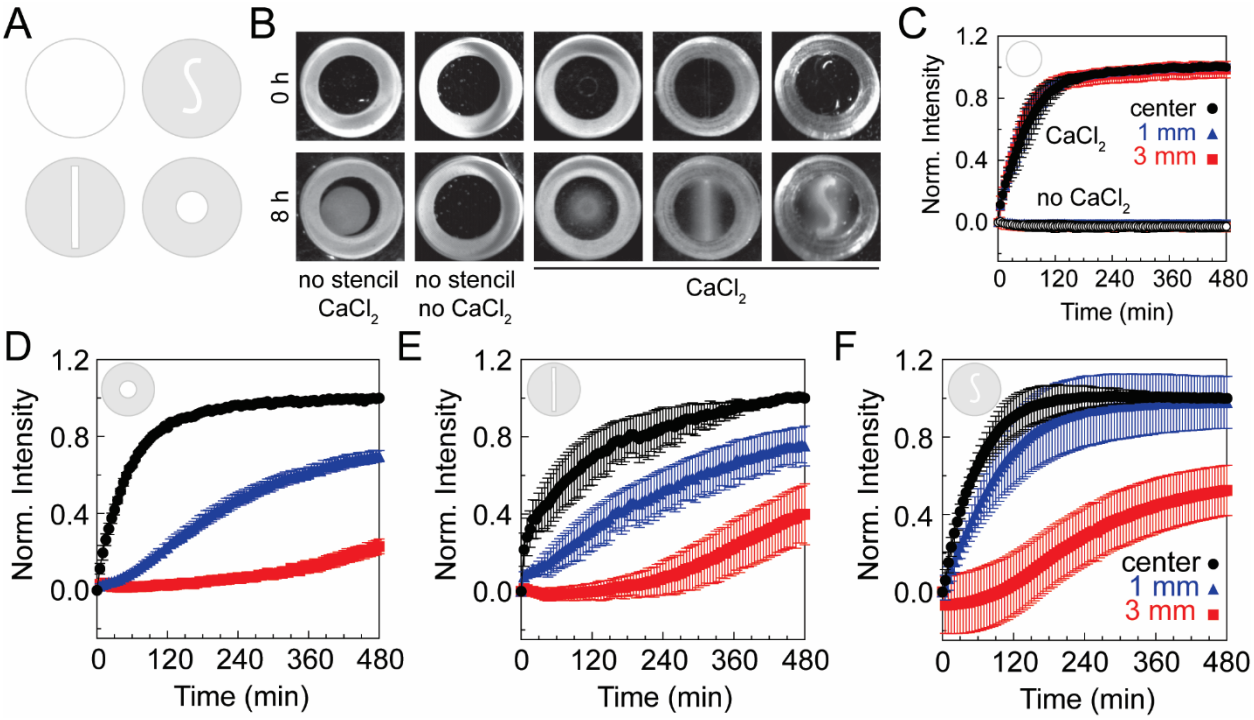

Figure 3: Stencil shape and exposure time determine the opacity gradient in alginate gels. A) Schematic of the unique stencils used to create gradients in opacity within the alginate gels. B) Representative images of alginate gels (20 mg/ml alginate cross-linked with 20 mM $CaSO_4$) before (0 h) and after (8 h) exposure to an 80 mM $CaCl_2$ solution above the stencil. Images are 25.4 mm by 25.4 mm. C) Normalized intensity over time with no stencil on the alginate gels and with and without 80 mM $CaCl_2$ at the center (black circles), 1 mm (blue triangles) and 3 mm (red squares) from the edge of the stencil (N_{days} = 3, N_{gels} = 3, $N_{points,\ center}$ = 3 and $N_{points,\ 1\ mm\ or\ 3\ mm}$ = 6). Normalized intensity over time for the D) circle stencil (N_{days} = 2, N_{gels} = 5, $N_{points,\ center}$ = 5 and $N_{points,\ 1\ mm\ or\ 3\ mm}$ = 10), E) line stencil (N_{days} = 5, N_{gels} = 5, $N_{points,\ center}$ = 5 and $N_{points,\ 1\ mm\ or\ 3\ mm}$ = 10) and F) S-shaped stencil (N_{days} = 5, N_{gels} = 5, $N_{points,\ center}$ = 5 and $N_{points,\ 1\ mm\ or\ 3\ mm}$ = 10) at distances 0 (center), 1, 3 mm from the center of the gel. Error bars represent 95% confidence intervals.

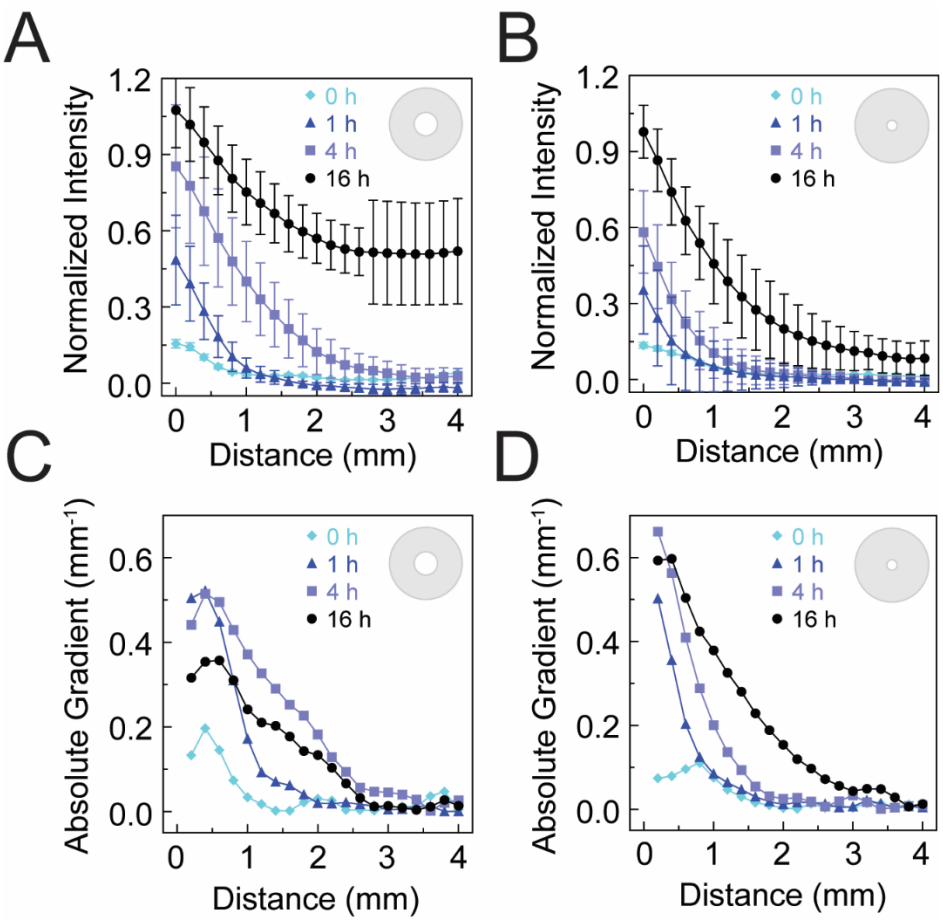

Figure 4: Stencil shape determines the kinetics of opacity gradient development in alginate gels. Normalized intensity within an alginate gel (20 mg/ml alginate cross-linked with 20 mM $CaSO_4$) as a function of radial distance from the edge of the opening in a A) 5 mm diameter stencil (N_{gels} = 8, N_{days} = 8) and a B) 2.5 mm diameter stencil (N_{gels} = 8, N_{days} = 6) after exposure to an 80 mM $CaCl_2$ solution above the stencil. Absolute gradient calculated as the slope of the normalized intensity over radial distance for C) the 5 and D) 2.5 mm diameter circle stencil. Error bars represent 95% confidence intervals.

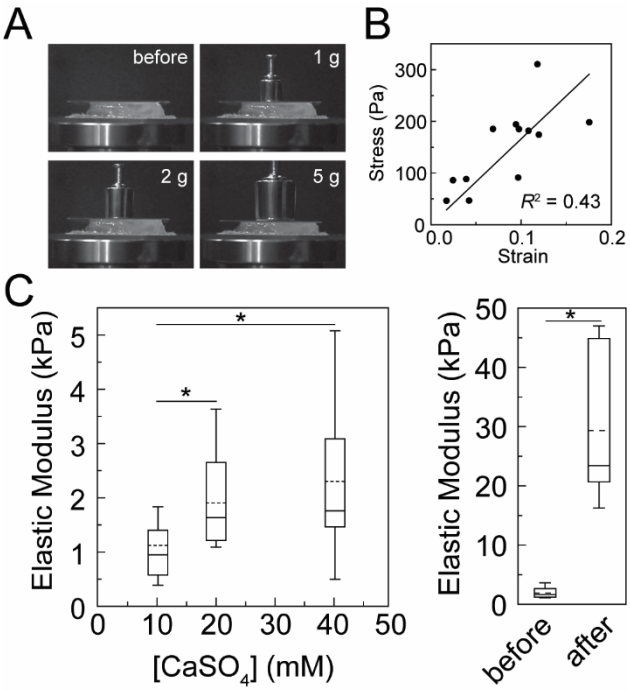

Figure 5: Increasing concentrations of calcium increase elastic modulus of alginate gels. A) Representative images of uniaxial compression testing of alginate hydrogels with different weights. B) Representative stress (σ) vs strain (γ) curve where the slope is equal to the elastic modulus. Elastic modulus was calculated as follows: $\sigma = E\gamma$. C) The elastic modulus of 20 mg/ml alginate hydrogels cross-linked with different concentrations of $CaSO_4$ and no $CaCl_2$. D) Elastic modulus of 20 mg/ml alginate and 20 mM $CaSO_4$ hydrogels before and after (22 h) adding 80 mM $CaCl_2$. No stencils were used. $N_{gels,\ 10\ mM} = 14$, $N_{gels,\ 20\ mM} = 22$, $N_{gels,\ 40\ mM} = 18$, $N_{gels,\ 20\ mM\ to\ 80\ mM} = 7$ independent gels. Box plots: Upper and lower error bars are minimum and maximum values, top and bottom of the box represent the 75th and 25th percentile, the line is the median and the dashed line is the mean. Conditions that resulted in *t*-tests with $p < 0.05$ are denoted with asterisks.

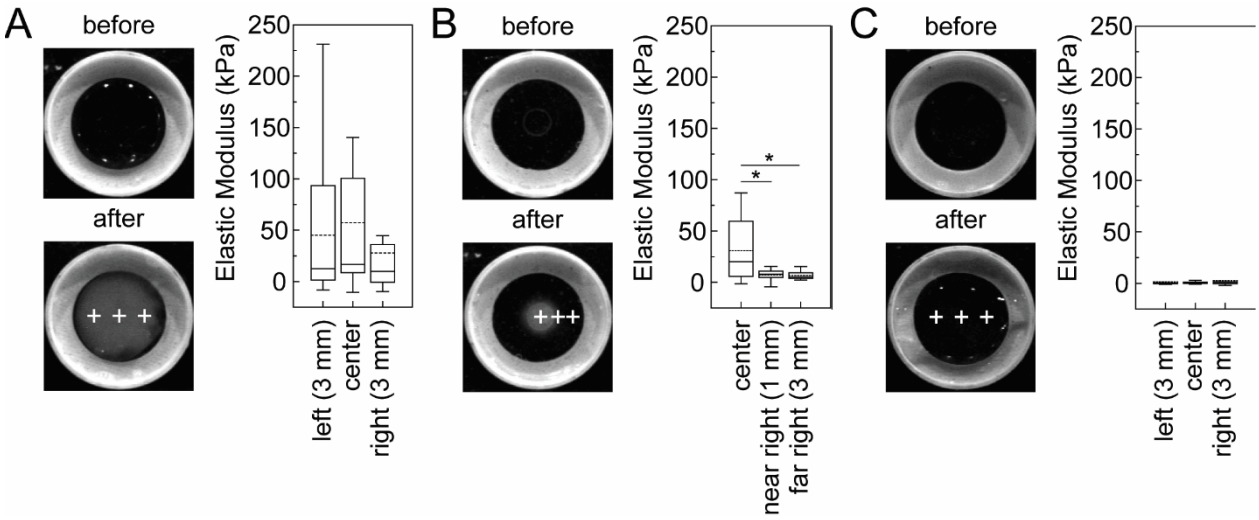

Figure 6: Stencils can create spatial mechanical property gradients in alginate gels. Imaging and mechanical property measurements were conducted on alginate gels (20 mg/ml alginate cross-linked with 20 mM $CaSO_4$) that were A) exposed to a solution of 80 mM $CaCl_2$ with no stencil, B) exposed to a solution of 80 mM $CaCl_2$ above a 5 mm circular stencil or C) 60 mM NaCl for 3 h. Images were recorded before and after exposure to the solution. Mechanical properties were assessed at different positions denoted by the crosses in the image. Images are 25.4 mm by 25.4 mm. The 80 mM $CaCl_2$ no stencil condition mechanical properties were determined from four days of experiments on four different gels probed at least three different times (N_{left} = 12, N_{center} = 13, N_{right} = 13). The 80 mM $CaCl_2$ stencil condition mechanical properties were determined from three days of experiments on three different gels probed at least three different times (N_{center} = 14, $N_{near\ right}$ = 10, $N_{far\ right}$ = 9). The 60 mM NaCl no stencil condition mechanical properties were determined from two days of experiments on two different gels probed at least three different times (N_{left} = 12, N_{center} = 9, N_{right} = 7). Box plots: Upper and lower error bars are minimum and maximum values, top and bottom of the box represent the 75th and 25th percentile, the line is the median and the dashed line is the mean. Conditions that resulted in *t*-tests with $p < 0.05$ are denoted with asterisks.

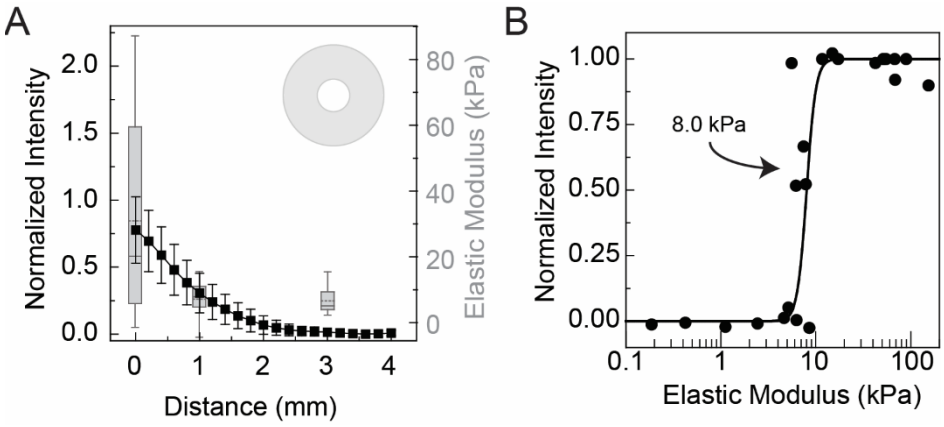

Figure 7: Opacity correlates with elastic modulus. A) Alginate gels (20 mg/ml alginate cross-linked with 20 mM $CaSO_4$) were exposed to a solution of 80 mM $CaCl_2$ with a 5 mm diameter circular stencil (top right) for 3 h and the opacity was measured (black squares, left) along with the elastic modulus (grey box plot, right) at different distances from the stencil edge. Error bars represent 95% confidence intervals. Box plots: Upper and lower error bars are minimum and maximum values, top and bottom of the box represent the 75th and 25th percentile, the line is the median and the dashed line is the mean. B) Opacity is plotted as a function of elastic modulus for positions in alginate gels (20 mg/ml alginate cross-linked with 20 mM $CaSO_4$) that were exposed to a solution of 80 mM $CaCl_2$ with no stencil, exposed to a solution of 80 mM $CaCl_2$ above a 5 mm circular stencil or 60 mM NaCl for 3 h. The model is an empirical sigmoidal fit with the half max shown.

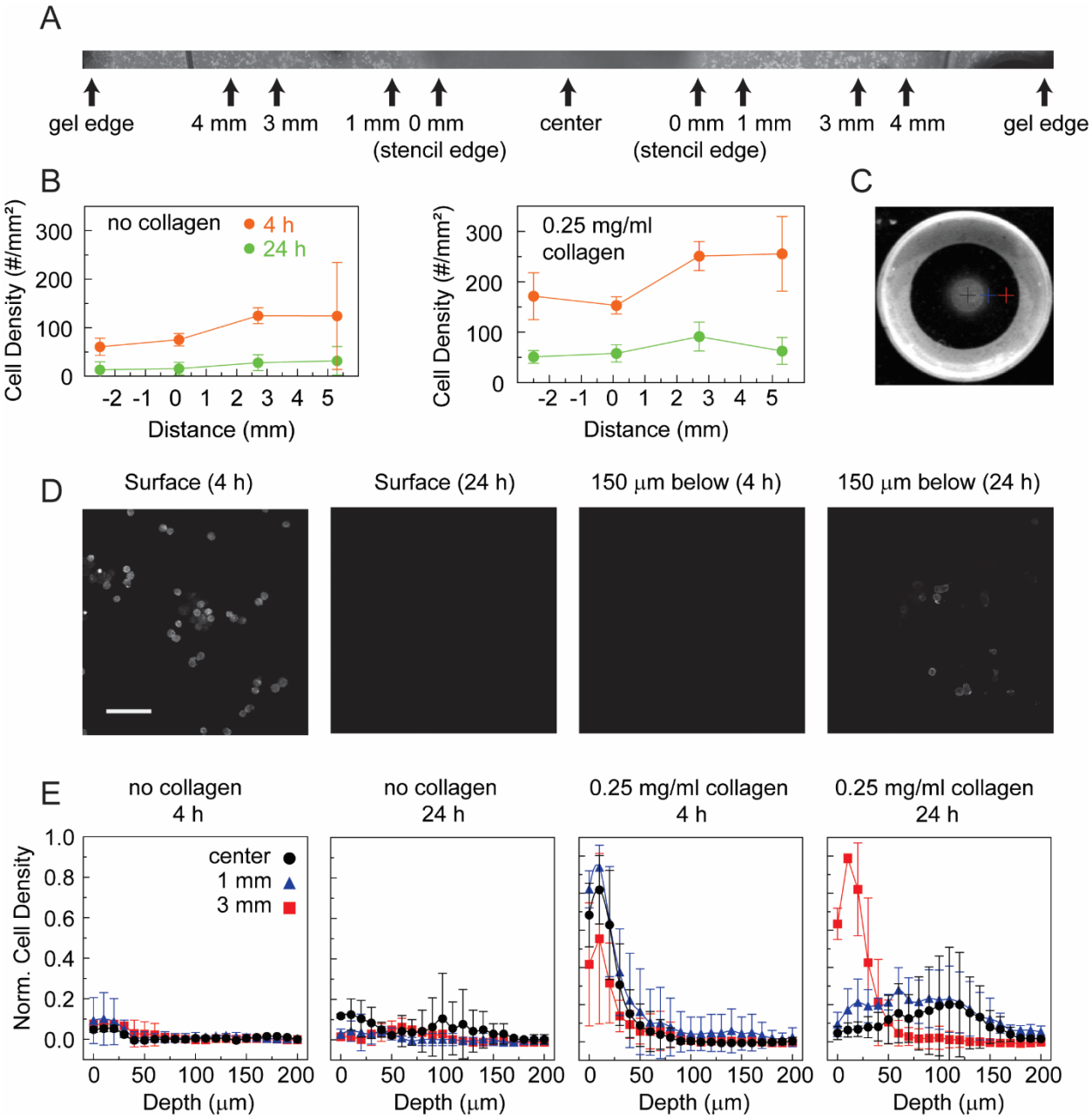

Figure 8: Stiffness gradients create a gradient in cancer cell invasion efficiency. Breast cancer cells (MDA-MB-231) were plated on the surface of collagen functionalized alginate gels with spatial stiffness gradients. A) Phase contrast images were taken and stitched across the entire gel. Positions where measurements were taken and reported are marked. B) Cell attachment density was quantified at different positions by examining the stitched images of alginate gels with and without collagen functionalization at both early (4 h) and late (24 h) timepoints. (no collagen: $N_{days} = 2$, $N_{gels} = 3$, $N_{points} = 6$, collagen: $N_{days} = 2$, $N_{gels} = 4$, $N_{points} = 8$) C) Image of the alginate gel is marked at different positions denoted by the crosses to indicate where invasion was assessed. Images are 25.4 mm by 25.4 mm. D) Confocal fluorescence images

were taken of cells fixed and stained with phalloidin on alginate gels functionalized with collagen in the center of the gel at different times and at different depths. The scale bar is 100 μm. E) Normalized cell density was quantified for alginate gels with and without collagen functionalization measured at the center of the gel (black circles), 1 mm from the stencil edge (blue triangles) and 3 mm from the stencil edge (red squares) at different depths (no collagen: $N_{days} = 2$, $N_{gels} = 2$, $N_{points} = 2$, collagen: $N_{days} = 2$, $N_{gels} = 3$, $N_{points} = 4$). Error bars are 95% confidence intervals.

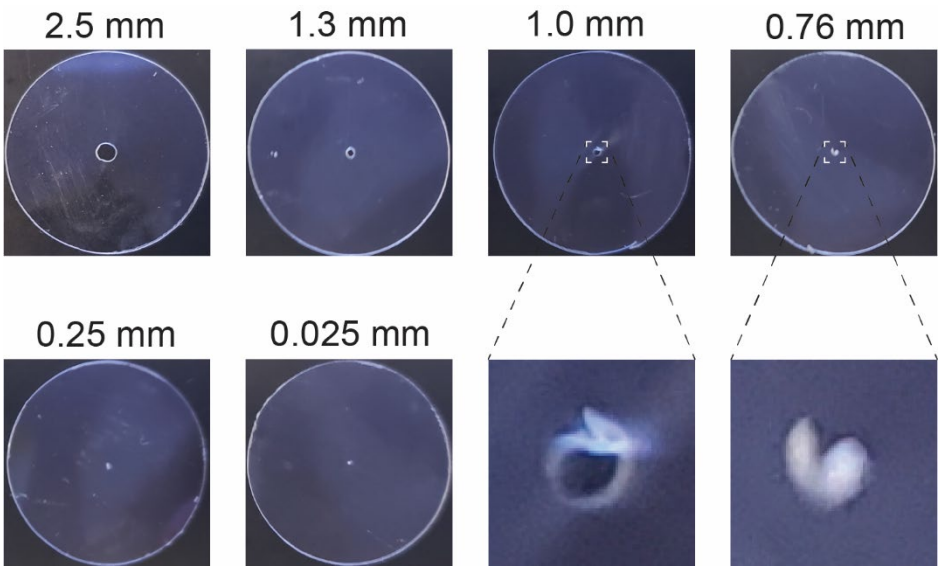

Supplementary Figure 1: Craft cutter stencil cutting resolution. Circles of various diameters were cut into the stencil material. Enlarged regions of selected stencils are shown. Images are 25.4 mm by 25.4 mm.

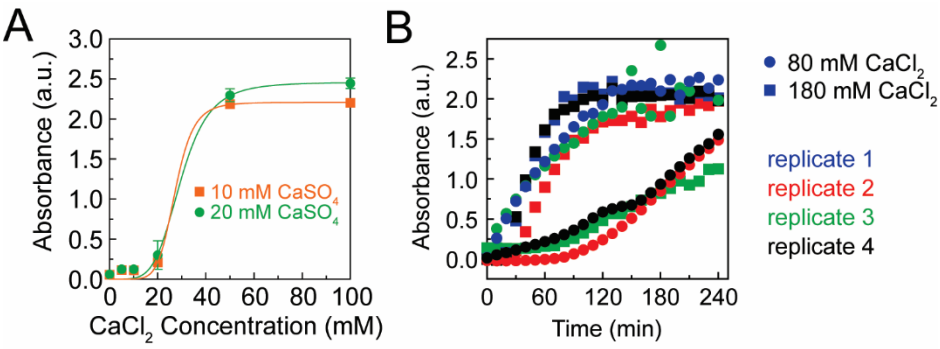

Supplementary Figure 2: Measuring kinetics of alginate polymerization using absorbance. A) Dose response of the absorbance at 750 nm of an alginate gel (20 mg/ml alginate) sparsely cross-linked with 20 mM $CaSO_4$ (green) or 10 mM $CaSO_4$ (orange) as a function of exposure to different concentrations of $CaCl_2$ after 16-24 h (N_{gels} = 3-5). Error bars represent 95% confidence intervals. B) Absorbance at 750 nm of alginate gels (20 mg/ml alginate cross-linked with 20 mM $CaSO_4$) after exposure to 80 or 180 mM $CaCl_2$ as a function of time.

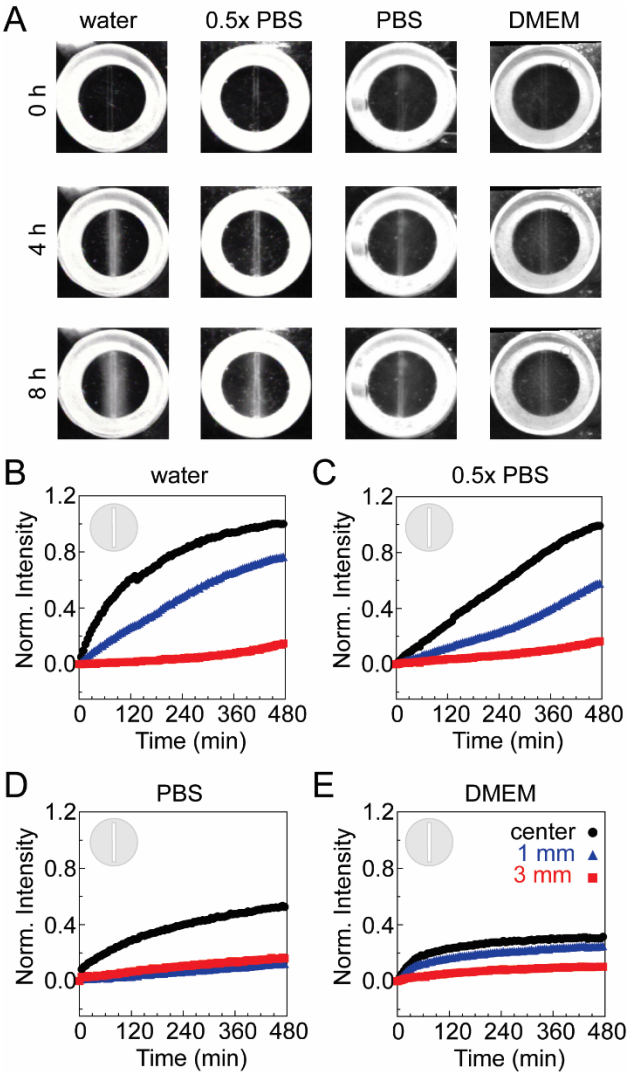

Supplementary Figure 3: Gradients in opacity produced in other buffers. A) Images of alginate gels (20 mg/ml alginate cross-linked with 20 mM $CaSO_4$) in different buffers (water, 0.5X PBS, PBS and DMEM) at various times (0, 4 and 8 h) after exposure to an 80 mM $CaCl_2$ solution in different buffers (water, water, PBS and DMEM) above the stencil. Images are 25.4 mm by 25.4 mm. Normalized intensity over time of gels in B) water, C) 0.5x PBS, D) PBS and E) DMEM with a line stencil on the alginate gels at distances of 0 (center), 1 and 3 mm from the center of the gel.

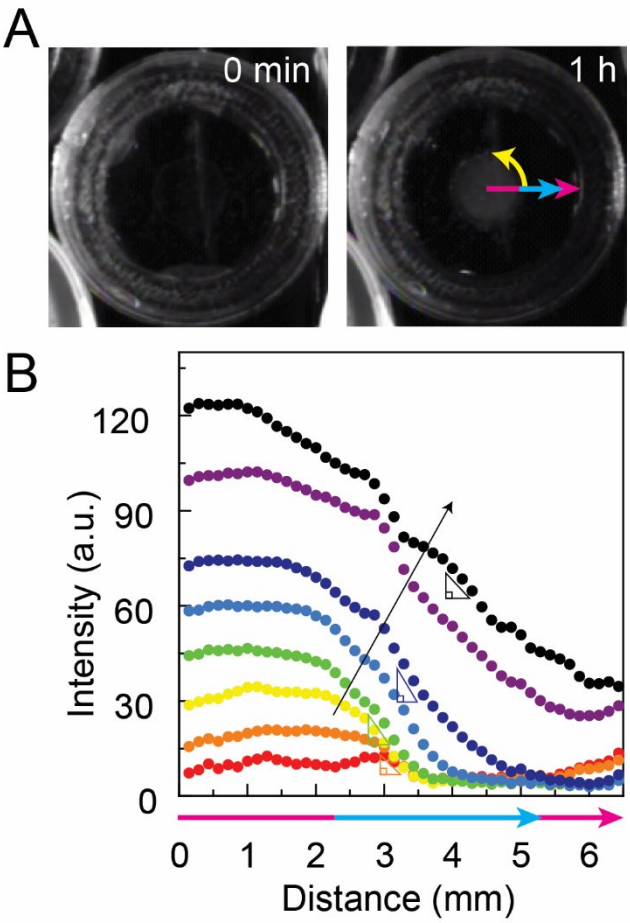

Supplementary Figure 4: Description of analysis approach to quantify the opacity radial profile. A) Representative images of alginate gels (20 mg/ml alginate cross-linked with 20 mM $CaSO_4$) before (0 h) and after (1 h) exposure to an 80 mM $CaCl_2$ solution above the stencil. The entire radial linescan (magenta arrow), the radial linescan used for data analysis (blue arrow) and the direction of angle sweep to average the radial opacity profile over all angles. Images are 25.4 mm by 25.4 mm. B) Normalized intensity averaged over all angles as a function of distance at various times ranging from short times (0 h, red) to long times (16 h, black). Triangles represent where an absolute gradient is calculated for a specific position.

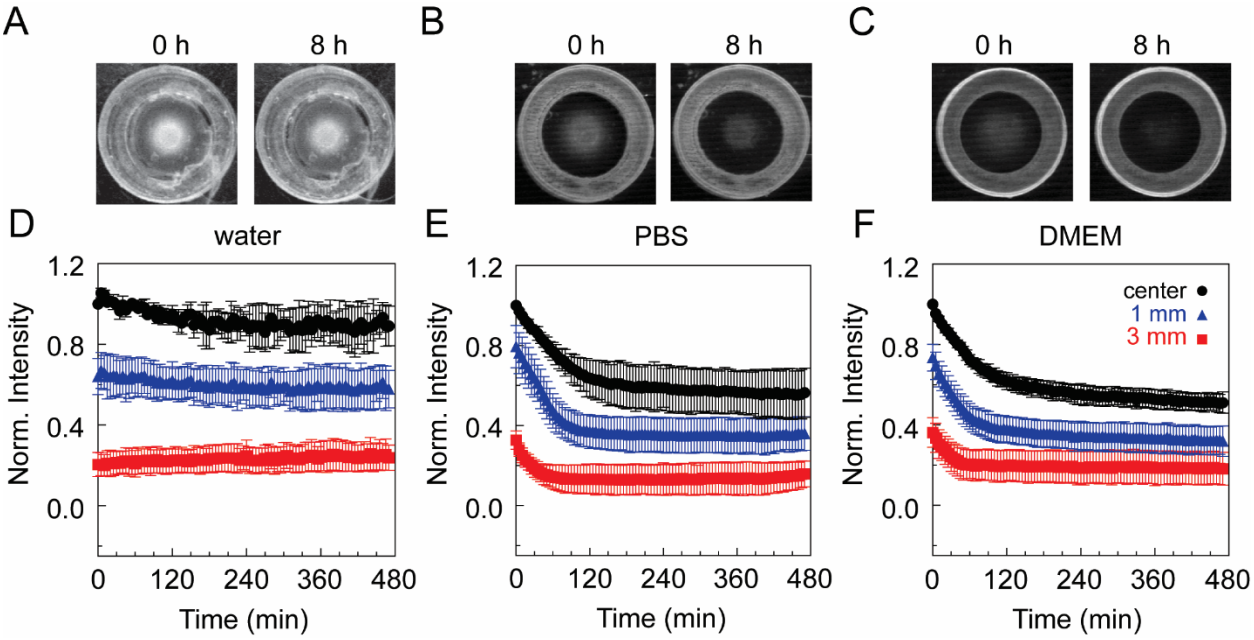

Supplementary Figure 5: Measuring opacity changes after removal of calcium from solution above gels. Representative images of alginate gels (20 mg/ml alginate cross-linked with 20 mM $CaSO_4$) after 8 h exposure to an 80 mM $CaCl_2$ solution above the stencil (marked as 0 h) and subsequent exposure to A) water, B) PBS or C) DMEM (marked as 8 h). Images are 25.4 mm by 25.4 mm. Normalized intensity over time at distances of 0 (center), 1 and 3 mm from the center of the gel in D) water (N_{days} = 2, N_{gels} = 3, $N_{points,\ center}$ = 3, $N_{points,\ 1mm\ or\ 3mm}$ = 6), E) PBS (N_{days} = 2, N_{gels} = 3, $N_{points,\ center}$ = 3, $N_{points,\ 1mm\ or\ 3mm}$ = 6) and F) DMEM (N_{days} = 2, N_{gels} = 4, $N_{points,\ center}$ = 4, $N_{points,\ 1mm\ or\ 3mm}$ = 8). Error bars represent 95% confidence intervals.

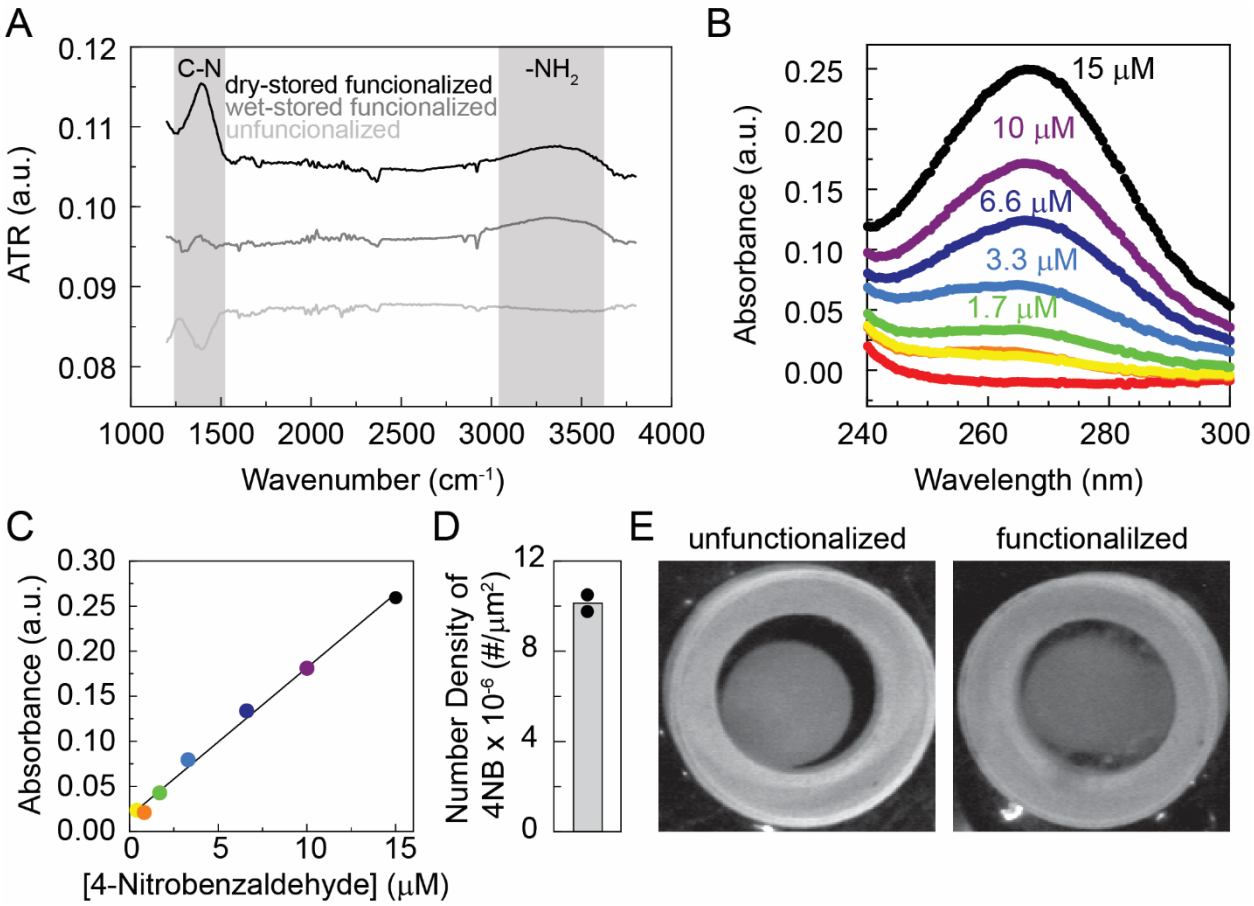

Supplementary Figure 6: Characterization of functional attachment of alginate to glass. A) ATR signal from FTIR spectroscopy of functionalized borosilicate glass kept dry or wet and unfunctionalized glass. Probable functional groups that cause the largest peaks in the ATR are denoted above. B) Absorbance scan of different concentrations of 4-nitrobenzaldehyde (red is 0 μM). C) Calibration curve generated by measuring absorbance at 270 nm as a function of 4NB concentration with a linear fit. D) Quantification of number density of amine groups as calculated by the amount of 4-nitrobenzaldehyde (4NB) hydrolyzed from the surface. The black dots represent two independent experiments and the grey bar is the mean. E) Representative images of alginate gels (20 mg/ml alginate cross-linked with 20 mM $CaSO_4$) after 8 h exposure to an 80 mM $CaCl_2$ solution on either unfunctionalized glass or functionalized glass. Images are 25.4 mm by 25.4 mm.

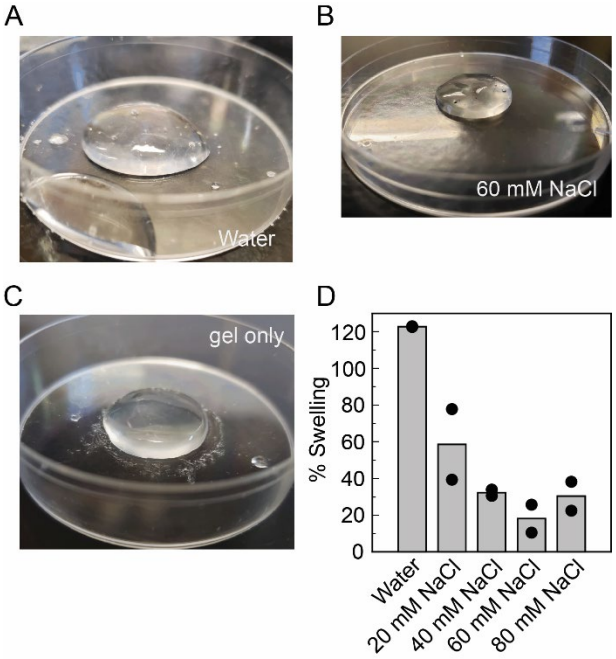

Supplementary Figure 7: Swelling of alginate gels in different buffers. Representative images for alginate gels (20 mg/ml alginate crosslinked with 20 mM $CaSO_4$) made in a 60 mm dish A) after exposure to water for 12 h, B) after exposure to 60 mM NaCl for 12h and C) initially at time 0 h. D) The average percent swelling (grey bars) and individual sample percent swelling (black circles) calculated at the mass of additional water in the gel divided by the initial mass of the gel x 100%.

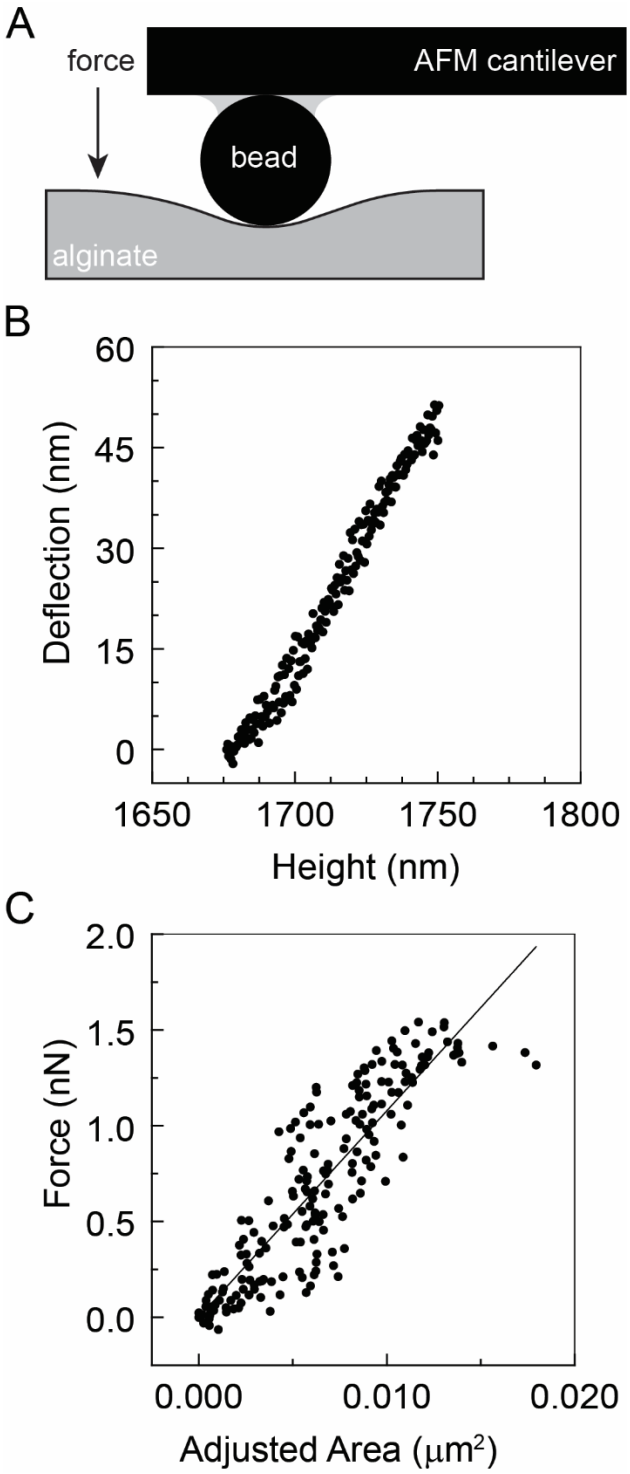

Supplementary Figure 8: Measurement of elastic modulus using atomic force microscopy. A) Schematic showing the deformation experiment using AFM. B) Sample graph of cantilever deflection as a function of height. C) Sample graph of force as a function of adjusted area, where the slope is the Young's modulus of the material.